Applied Mathematical Modelling 143 (2025) 116038

Contents lists available at ScienceDirect

Applied Mathematical Modelling

journal homepage: www.elsevier.com/locate/apm

Experimental observer-based delayed control of wheeled mobile robots ☆,☆☆

Jesús Abraham Rodríguez-Arellano [a], Roger Miranda-Colorado [b,*], Raúl Villafuerte-Segura [c], Luis T. Aguilar [a]

[a] Instituto Politécnico Nacional, Centro de Investigación y Desarrollo de Tecnología Digital, Av. Instituto Politécnico Nacional, No. 1310, Nueva Tijuana, Tijuana, Baja California, 22435, Mexico
[b] SECIHTI-Centro de Investigación y de Estudios Avanzados del Instituto Politécnico Nacional, Cinvestav, Unidad Zacatenco, Departamento de Control Automático, Av. Instituto Politécnico Nacional No. 2508, Col. San Pedro Zacatenco, Mexico City, 07360, Mexico
[c] Centro de Investigación en Tecnologías de Información y Sistemas, Universidad Autónoma del Estado de Hidalgo, Pachuca-Hidalgo, CP 42184, Mexico

ARTICLE INFO

Keywords:
Wheeled mobile robot
Delays
Proportional-retarded control
Disturbance observer
Experimental platform

ABSTRACT

Wheeled mobile robots are essential mechatronic systems that have attracted attention in different applications in industry and for research. One essential task commanded to a wheeled mobile robot is following a desired reference signal. However, in practical situations, wheeled mobile robots are always affected by disturbances diminishing the closed-loop performance. Hence, this manuscript develops a novel robust control scheme that allows accomplishing a trajectory-tracking task including disturbances. A disturbance observer is designed to compensate for disturbances in the proposed methodology. Also, the delay theory is used to design a proportional-retarded controller that makes the wheeled mobile robot's position and orientation signals converge to their desired references asymptotically. A theoretical development proves the effectiveness of the new scheme. The novel methodology is compared against other robust control methodologies from the literature. Various experiments on a scaled vehicle demonstrate that the novel controller outperforms the other robust controllers, thus representing a viable choice for controlling wheeled mobile robots.

1. Introduction

In recent years, the scientific and technological community has paid particular attention to the generation of interfaces and algorithms that assist in designing, constructing, and controlling mobile robots. A mobile robot is a system that requires knowledge and implementation of basic sciences and engineering such as mathematics, physics, mechanics, electronics, and computing, among others. They are essential within the field of mechatronic systems, which share some technical problems with other types of robots but

☆ This work was supported by Secretaría de Ciencia, Humanidades, Tecnología e Innovación (SECIHTI), Project "Control Robusto para el Control y Reducción de Consumo Energético de Sistemas Mecatrónicos", CIR/063/2024.
☆☆ The author declares that there is not conflict of interest regarding the publication of this paper.
* Corresponding author.
E-mail address: rmirandaco@secihti.mx (R. Miranda-Colorado).

https://doi.org/10.1016/j.apm.2025.116038
Received 8 November 2024; Received in revised form 19 February 2025; Accepted 20 February 2025

Available online 21 February 2025

also have their own difficulties regarding their movement and adaptation in real-world scenarios [1,2]. One way to classify mobile robots is based on their locomotion and operating environment [3].

Wheeled mobile robots (WMRs) are a type of mobile robots that can be classified according to their type of wheels (e.g., conventional wheels such as fixed wheel, castor wheel, powered steering wheel without offset, power steering wheel with longitudinal offset, or special wheels such as universal wheel [4], mecanum wheel [5], or ball wheel [6]) [7].

According to the vehicle configuration, there are two main WMR classifications: The unicycle-type and Ackerman-type mobile robots [8–11]. An Ackerman mobile robot is a four-wheeled vehicle similar to a car, also known as a car-like robot. Numerous control strategies have been developed for the unicycle model [12–14]. However, these schemes cannot be applied to the car-like model due to differences in their control requirements. The unicycle model involves three generalized variables, whereas a car-like robot requires managing four variables, hence becoming more complex for control purposes. From now on, the car-like robot model will be referred to as the complete kinematic model and the unicycle robot model as the simplified kinematic model. In this work, car-like robots are our case of study and will be referred to as wheeled mobile robots (WMRs).

There has been a growing generation of knowledge around car-like robots, mainly due to the need to automate the vehicles of everyday life. However, unlike manipulator arms or other wheeled mobile robots, these robots are not capable of moving the vehicle forward or backward in a direction perpendicular to the orientation of the rear wheel rotation axis [15]. Therefore, designing and tuning controllers for these types of vehicles is a non-trivial task.

WMRs have various applications, such as planetary exploration, autonomous driving, entertainment, exploration of narrow areas, formation control, and agriculture [16–19]. However, WMRs have inherent challenges, such as complexity due to their nonlinearities and having fewer control inputs than controllable variables, making them underactuated. Additionally, their kinematic model is subject to nonholonomic constraints [20]. Besides, it is impossible to avoid disturbances in real-world scenarios, making these systems challenging to control. Thus, research in the field of WMRs is essential and deserves further study.

The main tasks to be addressed in controlling WMRs are path tracking, point stabilization, and trajectory tracking. Path tracking involves controlling the WMR's position at a specified speed; point stabilization focuses on aligning the robot's position to a predetermined point; and trajectory tracking seeks to follow a path while incorporating time as a parameter, allowing the robot to reach a desired location within a given time [3,21]. This work will focus on trajectory-tracking tasks due to their importance in specific scenarios where it is required to reach a desired position within a specific time [22–24]. Additionally, the movement limitations imposed by nonholonomic constraints make control design for car-like robots more complex, limiting the trackable trajectories [25,26]. However, a feasible trajectory must account for these kinematic restrictions. Hence, the reference kinematic model must ensure its successful implementation [21,27].

Referring to the controller design stage, reference [28] proposes robust controllers against parametric uncertainties, mass variations, electrical parameters, and external perturbations. In [29], the need to predict wheel-soil interaction performance from knowledge of terra mechanics is discussed, which is essential for controlling planetary rovers. The design of a variable frame tracking controller for a mobile robot system using a dynamic oscillator and a Lyapunov-based stability analysis is presented in [30]. From a control design perspective, a kinematic model for a WMR in the presence of wheel slipping and skidding is presented in [31]. Also, in [32], a quantized feedback tracker design problem for nonholonomic mobile robots with uncertain nonlinear dynamics in a network environment with state and input quantization is analyzed. In [33], a controller that allows the WMR to move in a dynamic and partially known environment with autonomous movement capabilities is proposed. The design of a nonlinear adaptive control law to preserve accuracy in agricultural applications of farm vehicles is presented in [34]. An interesting Takagi-Sugeno fuzzy-model-based approach is developed in [35] using visual odometry, proving the validity of the proposed scheme through a Lyapunov analysis.

Currently, there are different approaches in which trajectory tracking has been tackled, including Sliding Mode Control (SMC) [36,37], feedback schemes [16,21,38], observer-based [39,40], and intelligent approaches [20,41]. For the feedback techniques, De Luca and collaborators [21] designed controllers for the complete WMR's kinematic model using both exact and approximate feedback linearization techniques, showing good tracking performance with a simple control structure; nevertheless, the stability analysis does not account for disturbances which do not provide robustness. Yan and collaborators [42] designed an exciting scheme that employs a coordinate transformation to obtain a decoupled system and design an observer-based feedback controller; this scheme uses position and velocity measurements; besides, the response exhibited attains fast convergence; however, the unicycle kinematic model was employed.

Regarding intelligent approaches, Liu and collaborators [43] proposed an adaptive Neural Network methodology by employing the complete WMR's kinematic model; this scheme has good tracking response despite disturbances; however, it does not include tracking errors of the generalized coordinates. In [44], two PID controllers were employed for trajectory tracking while considering the dynamic model and a Neural Network to generate the trajectory and avoid obstacles; nonetheless, the authors used the simplified kinematic model, and the simulation results exhibit a low tracking response.

SMC methodologies are relevant due to their inherited robustness property of dealing with matched disturbances and, in some cases, attaining finite time stability. Vilchis and collaborators [45] developed a controller employing the complete kinematic model through a decoupling approach, which exhibits a good tracking response; however, this approach does not consider disturbances in the stability analysis. In [36], a novel observer-based SMC controller is designed using the complete WMR's model description; the results demonstrate good tracking response and robustness due to the SMC and the observer employed for matched disturbances; however, the transient response exhibits oscillations, which is undesirable in real scenarios.

Other methodologies focus on fast response by ensuring fixed time and prescribed time stability. Reference [46] proposes an interesting approach by designing a fault-tolerant prescribed performance control that employs a barrier function to reach a neighborhood near the origin in prescribed time while considering disturbances; the authors employed the simplified kinematic model,

attaining low steady-state error; however, the transient response is slow, and the control design stage is convoluted, which affects the tuning stage that could yield into poor performance. Furthermore, in [47], a decoupling approach was proposed while considering kinematic disturbances; nevertheless, the unicycle model was employed, the convergence rate was low, and the controller structure was complex. An adaptive fuzzy controller with a prescribed trajectory performance was developed in [48]; the authors designed the controller with a simple structure which allows the designer to preset the upper bound of the tracking error a priori and the settling time; nevertheless, the kinematic and dynamic models employed are from the unicycle vehicle, the convergence is slow, and the tracking errors of the generalized coordinates are not provided. Another approach employing the complete kinematic model is reported in [49], where the system was decoupled, which allowed the design of a backstepping controller coupled with an extended state observer to estimate kinematic disturbances; the results exhibit a fast response to the desired control signals and low tracking errors; however, no data are showing the tracking errors of the complete kinematic model and exist oscillations on the front wheel's steering angle.

From the previous study, it is clear that to implement a controller, knowing the complete vehicle's state is required; however, sometimes this is not possible due to non-measurable state variables. Therefore, the implementation of observers is necessary. In this sense, some works dealing with this issue include [50], where a comparison between a linear and a non-linear observer is presented for the side-slip angles of the car-like vehicles and tire side-slip angles. In [51], the state of the automobile-type tractor necessary for control is estimated by developing a non-linear observer, which only uses information from sensors mounted on the vehicle. Reference [52] proposes a fault diagnosis scheme using a higher-order sliding mode observer and a reconfigurable controller based on the super-twisting algorithm.

In real scenarios, we always face noisy measurements in WMRs due to sensors or actuators. These noises are usually increased in the control stage, causing sustained damage to the actuators, malfunctions, and undesirable behavior in the closed-loop system response. An efficient way to mitigate noises in the control stage is to use a delayed action controller or delayed controller, that is, to use artificial time delays [53]. Some other studies claim that it is more convenient to replace a derivative action with a delayed action in the control law [54]. Also, the delayed controllers are easy to implement in practical applications, such as mechatronic/robotic systems [55–57]. Furthermore, serious studies found in the literature have shown that using time delays in the control law improves the closed-loop performance since an exponential decay bound on the convergence of the response can be guaranteed [58]. Hence, a delayed action in the controller design stage may improve the closed-loop system performance. Therefore, in this work, we propose a new control scheme that encompasses an observer with a delayed controller.

1.1. Contribution

The previous study shows the main drawbacks and gaps needing further study. Specifically, these issues include: low convergence rate, not including the effect of the disturbances when designing the controller, the existence of oscillations in the system's closed-loop signals, the impact of measurement noise in the system's performance, the complexity of the controllers applied to WMRs, and considering a simplified WMR's kinematic description [46,59,60]. Then, this work aims to overcome the abovementioned issues by developing an observer-based proportional-retarded controller that accomplishes the trajectory-tracking task. In the proposed methodology, the controller is split into two main parts:

- A disturbance observer is designed to compensate for disturbances. It transforms the original system into other with vanishing disturbances.
- A proportional retarded controller that makes the position and orientation signals converge to their desired references despite disturbances. This controller uses the spectral abscissa approach and the σ-stability regions to include artificial delays in its structure and guarantee the maximum decay rate σ in the closed-loop system response.

Extensive experiments demonstrate the feasibility of the new controller. In addition, other robust control methodologies are used to validate the performance of the new methodology. Experimental results demonstrate the outstanding and better efficiency of the novel controller over the other techniques from the literature. Besides, the new methodology allows for attaining asymptotic stability. Hence, the main contributions of this work are:

- Developing a novel observer-based proportional-retarded methodology to control a WMR in trajectory-tracking tasks. This scheme also has a simple mathematical structure.
- A theoretical development proving the efficiency of the new control scheme is included. Besides, robustness against disturbances is proved.
- Performing experiments on a scaled vehicle, proving the validity of the theoretical results developed in this manuscript. Moreover, the fast convergence of the new control scheme is verified when compared against other methodologies.
- Including an extensive experimental analysis with other robust control methodologies, demonstrating that the new scheme surpasses the robust controllers used for comparison.

1.2. Organization

The WMR's mathematical description and the problem under study are presented in Section 2. The theoretical analysis, including the design of the disturbance observer and the proportional-retarded controller, is presented in Section 3. Then, extensive experimental

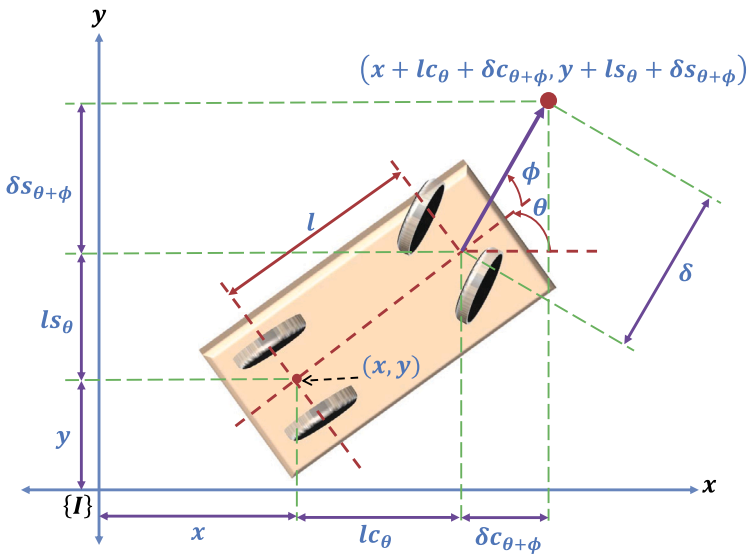

Fig. 1. General diagram of a WMR and its corresponding coordinates $\boldsymbol{q}^T = [x, y, \theta, \phi]$.

results are presented in Section 4. Here, the controllers used for comparison are mathematically described. Then, qualitative and quantitative data are used to demonstrate the superior performance of the novel control scheme. Finally, this manuscript presents some conclusions and future studies in Section 5.

1.3. Notation

This document considers $\mathbb{R}$ as the real numbers; $|\cdot|$ and $\|\cdot\|$ are the absolute value and the Euclidean norm operators; we have the signum function $\text{sign}(\vartheta) = \vartheta/|\vartheta|$ if $\vartheta \neq 0$, $\text{sign}(0) \in [-1, 1]$. Vectors are expressed as bold lowercase letters, while matrices are referred to with uppercase letters. Also, s_φ, c_φ, and t_φ correspond to the functions $\sin(\varphi)$, $\cos(\varphi)$, and $\tan(\varphi)$.

2. WMR kinematic model and problem statement

Fig. 1 shows the general description of a WMR. This schematic representation includes the vehicle position (x, y) concerning the inertial reference frame $\{\boldsymbol{I}\}$; the angle measured with respect to axis $\boldsymbol{x}$ is the WMR's orientation $\theta(t)$; angle $\phi(t)$ denotes the steering angle; and l is the distance between the rear and frontal wheels.

The following control methodology is based on the subsequent WMR's kinematic model [36]

$$\dot{\boldsymbol{q}}(t) = S(\boldsymbol{q})\boldsymbol{v}(t) + \boldsymbol{d}(t), \tag{1}$$

where

$$S(\boldsymbol{q}) = \begin{bmatrix} c_\theta & s_\theta & \frac{t_\phi}{l} & 0 \\ 0 & 0 & 0 & 1 \end{bmatrix}^T \in \mathbb{R}^{4\times 2},$$

$$\boldsymbol{q}(t) = \begin{bmatrix} x(t) & y(t) & \theta(t) & \phi(t) \end{bmatrix}^T,$$

$$\boldsymbol{v}(t) = \begin{bmatrix} v_1(t) & v_2(t) \end{bmatrix}^T \in \mathbb{R}^2,$$

$$\boldsymbol{d}(t) = \begin{bmatrix} d_1(t) & d_2(t) & d_3(t) & d_4(t) \end{bmatrix}^T \in \mathbb{R}^4,$$

with $\boldsymbol{d}(t)$ representing the vector encompassing the disturbances affecting the system and the control inputs $v_1(t)$ and $v_2(t)$ denoting the linear forward and angular steering velocities driving the WMR, respectively.

Disturbances $d_i(t)$, $i = 1, ..., 4$, include kinematic disturbance effects (e.g., skidding and slipping) [31,61]. The subsequent analysis considers the following assumption.

Assumption 1 *(A1). There exist positive constants $\bar{v}_1$, $\bar{v}_2$, $\bar{\phi}$, $\bar{d}_i$, and $\bar{d}_{di}$, $i = 1, ..., 4$, such that*

- *The maximum linear velocity is bounded, i.e.,*

$$|v_1(t)| \leq \bar{v}_1, \tag{2}$$

- *The maximum angular velocity is bounded, i.e.,*

$$\left|v_2(t)\right| \leq \bar{v}_2, \tag{3}$$

- *Mechanical restrictions on the vehicle ensure that*

$$|\phi(t)| \leq \bar{\phi} < \pi/2, \tag{4}$$

- *Disturbances and their time derivatives are bounded, i.e.,*

$$\left|d_i(t)\right| \leq \bar{d}_i, \tag{5}$$

$$\left|\dot{d}_i(t)\right| \leq \bar{d}_{di}. \tag{6}$$

Remark 1. Boundedness on $d_i(t)$ and $\dot{d}_i(t)$ is a strong condition from a mathematical point of view. Nevertheless, from a practical point of view, as considered for the WMR, internal and external disturbances can be modeled as bounded Lipschitz continuous functions within the domain of interest [36,62]. Moreover, for a real WMR, the maximum linear and angular steering velocities are also bounded. Furthermore, mechanical restrictions make condition (4) feasible, i.e., the maximum allowable steering angle is mechanically restricted. Hence, based on condition (4), the model given in (1) has no singularities because the magnitude of $\phi(t)$ is less than $\pi/2$. Besides, Assumption **A1** is always satisfied with a real WMR, given the structure described in this manuscript.

A plausible reference trajectory for a WMR must evolve from a kinematic model having the subsequent structure [21]

$$\dot{\boldsymbol{q}}_d(t) = S(\boldsymbol{q}_d)\boldsymbol{v}_d(t), \tag{7}$$

where

$$S(\boldsymbol{q}_d) = \begin{bmatrix} c_{\theta_d} & s_{\theta_d} & \frac{t_{\phi_d}}{l} & 0 \\ 0 & 0 & 0 & 1 \end{bmatrix}^T,$$

$$\boldsymbol{q}_d(t) = \begin{bmatrix} x_d(t) & y_d(t) & \theta_d(t) & \phi_d(t) \end{bmatrix}^T,$$

$$\boldsymbol{v}_d(t) = \begin{bmatrix} v_{d1}(t) & v_{d2}(t) \end{bmatrix}^T,$$

with $x_d(t)$, $y_d(t)$, $\theta_d(t)$, and $\phi_d(t)$ representing the desired position and orientation signals, and $\boldsymbol{v}_d(t)$ denotes the desired control input vector.

Now, let us consider $\boldsymbol{z}(t) \in \mathbb{R}^2$ as a new output and the desired output signal $\boldsymbol{z}_d(t)$, which are defined as follows

$$\boldsymbol{z}(t) = \begin{bmatrix} z_1(t) \\ z_2(t) \end{bmatrix} = \begin{bmatrix} x + lc_\theta + \delta c_{\theta+\phi} \\ y + ls_\theta + \delta s_{\theta+\phi} \end{bmatrix}, \tag{8}$$

$$\boldsymbol{z}_d(t) = \begin{bmatrix} z_{d1}(t) \\ z_{d2}(t) \end{bmatrix} = \begin{bmatrix} x_d + lc_{\theta_d} + \delta c_{\theta_d+\phi_d} \\ y_d + ls_{\theta_d} + \delta s_{\theta_d+\phi_d} \end{bmatrix}, \tag{9}$$

where $\delta \neq 0$ is a design constant parameter. Parameter δ can be understood as a decoupling factor. In a subsequent development, we utilize this parameter to transform the WMR description (7) into two perturbed second-order systems that simplify the controller design stage.

From equation (8)-(9), we obtain

$$\ddot{\boldsymbol{z}}(t) = A(\theta,\phi)\bar{\boldsymbol{u}}(t) + \bar{A}(t)\boldsymbol{v}(t) + \dot{\boldsymbol{\gamma}}_1(t), \tag{10}$$

$$\ddot{\boldsymbol{z}}_d(t) = A(\theta_d,\phi_d)\bar{\boldsymbol{u}}_d(t) + \bar{A}_d(t)\boldsymbol{v}_d(t). \tag{11}$$

Here

$$A(\theta,\phi) = \begin{bmatrix} a_{11} & a_{12} \\ a_{21} & a_{22} \end{bmatrix} = \begin{bmatrix} c_\theta - t_\phi\left(s_\theta + \frac{\delta}{l}s_{\theta+\phi}\right) & -\delta s_{\theta+\phi} \\ s_\theta + t_\phi\left(c_\theta + \frac{\delta}{l}c_{\theta+\phi}\right) & \delta c_{\theta+\phi} \end{bmatrix}, \tag{12}$$

$$\bar{A}(t) = \begin{bmatrix} \bar{a}_{11} & \bar{a}_{12} \\ \bar{a}_{21} & \bar{a}_{122} \end{bmatrix} = \begin{bmatrix} \dot{a}_{11} & \dot{a}_{12} \\ \dot{a}_{21} & \dot{a}_{22} \end{bmatrix}, \tag{13}$$

$$\boldsymbol{\gamma}_1 = \begin{bmatrix} \gamma_1 \\ \gamma_2 \end{bmatrix} = \begin{bmatrix} d_1(t) - ls_\theta d_3(t) - \delta s_{\theta+\phi}\left(d_3(t) + d_4(t)\right) \\ d_2(t) + lc_\theta d_3(t) + \delta c_{\theta+\phi}\left(d_3(t) + d_4(t)\right) \end{bmatrix}, \tag{14}$$

$$A(\theta_d,\phi_d) = \begin{bmatrix} a_{d11} & a_{d12} \\ a_{d21} & a_{d22} \end{bmatrix} = \begin{bmatrix} c_{\theta_d} - t_{\phi_d}\left(s_{\theta_d} + \frac{\delta}{l}s_{\theta_d+\phi_d}\right) & -\delta s_{\theta_d+\phi_d} \\ s_{\theta_d} + t_{\phi_d}\left(c_{\theta_d} + \frac{\delta}{l}c_{\theta_d+\phi_d}\right) & \delta c_{\theta_d+\phi_d} \end{bmatrix}, \tag{15}$$

$$\bar{A}_d(t) = \begin{bmatrix} \bar{a}_{d11} & \bar{a}_{d12} \\ \bar{a}_{d21} & \bar{a}_{d122} \end{bmatrix} = \begin{bmatrix} \dot{a}_{d11} & \dot{a}_{d12} \\ \dot{a}_{d21} & \dot{a}_{d22} \end{bmatrix}, \tag{16}$$

$$\bar{\boldsymbol{u}}(t) = \begin{bmatrix} u_1(t) & u_2(t) \end{bmatrix}^T = \begin{bmatrix} \dot{v}_1(t) & \dot{v}_2(t) \end{bmatrix}^T, \tag{17}$$

$$\bar{\boldsymbol{u}}_d(t) = \begin{bmatrix} u_{d1}(t) & u_{d2}(t) \end{bmatrix}^T = \begin{bmatrix} \dot{v}_{d1}(t) & \dot{v}_{d2}(t) \end{bmatrix}^T, \tag{18}$$

$$\dot{\boldsymbol{\gamma}}(t) = \begin{bmatrix} \dot{\gamma}_1(t) & \dot{\gamma}_2(t) \end{bmatrix}^T. \tag{19}$$

Based on the new output variables $\boldsymbol{z}(t)$ and $\boldsymbol{z}_d(t)$, we define the new tracking error signal $\tilde{\boldsymbol{z}}(t)$ as follows

$$\tilde{\boldsymbol{z}}(t) = \boldsymbol{z}(t) - \boldsymbol{z}_d(t). \tag{20}$$

By employing equations (10) and (11), $\ddot{\tilde{\boldsymbol{z}}}(t)$ yields the following differential equation describing the tracking error as follows

$$\ddot{\tilde{\boldsymbol{z}}}(t) = A(\theta,\phi)\bar{\boldsymbol{u}}(t) + \bar{A}(t)\boldsymbol{v}(t) + \dot{\boldsymbol{\gamma}}(t) - A(\theta_d,\phi_d)\bar{\boldsymbol{u}}_d(t) - \bar{A}_d(t)\boldsymbol{v}_d(t). \tag{21}$$

Now, let us define the states $x_i(t)$, $i = 1,...,4$, as follows

$$x_1(t) = \tilde{z}_1(t), \tag{22}$$

$$x_2(t) = \dot{\tilde{z}}_1(t), \tag{23}$$

$$x_3(t) = \tilde{z}_2(t), \tag{24}$$

$$x_4(t) = \dot{\tilde{z}}_2(t). \tag{25}$$

By utilizing (22)-(25), we transform (21) into the subsequent two perturbed second-order systems

$$\Sigma_1 \begin{cases} \dot{x}_1(t) = x_2(t), \\ \dot{x}_2(t) = u_1(t) + \sigma_1(t), \end{cases} \tag{26}$$

$$\Sigma_2 \begin{cases} \dot{x}_3(t) = x_3(t), \\ \dot{x}_4(t) = u_2(t) + \sigma_2(t), \end{cases} \tag{27}$$

where

$$\boldsymbol{u}(t) = \begin{bmatrix} u_1(t) & u_2(t) \end{bmatrix}^T = A(\theta,\phi)\bar{\boldsymbol{u}}(t), \tag{28}$$

$$\sigma_1(t) = \bar{a}_{11}v_1 + \bar{a}_{12}v_2 + \dot{\vartheta}_{11} - a_{d11}\dot{v}_{d1} - a_{d12}\dot{v}_{d2} - \bar{a}_{d11}v_{d1} - \bar{a}_{d12}v_{d2}, \tag{29}$$

$$\sigma_2(t) = \bar{a}_{21}v_1 + \bar{a}_{22}v_2 + \dot{\vartheta}_{22} - a_{d21}\dot{v}_{d1} - a_{d22}\dot{v}_{d2} - \bar{a}_{d21}v_{d1} + \bar{a}_{d22}v_{d2}. \tag{30}$$

Based on the previous second-order systems (26)-(27), we aim to develop a controller $\boldsymbol{u}(t) = [u_1(t), u_2(t)]^T$ that allows the reference signal $\boldsymbol{z}(t)$ to converge to the desired reference $\boldsymbol{z}_d(t)$ asymptotically. The control objective is given below.

Control objective. *Let the second-order systems (26)-(27). Then, $\boldsymbol{u}(t)$ will be designed to warrant that*

$$\lim_{t\to\infty} \boldsymbol{z}(t) = z_d(t). \tag{31}$$

Now, we have transformed the original WMR's kinematic model (1) into the two decoupled second-order systems (26)-(27). These systems are perturbed by the terms $\sigma_j(t)$, $j = 1,2$. Note that controlling the original nonlinear kinematic model is simplified through the transformation given by defining the new output signals $\boldsymbol{z}(t)$ and $\boldsymbol{z}_d(t)$ in equations (8)-(9). Then, in the following development, we provide a methodology that compensates for $\sigma_j(t)$, $j = 1,2$, transforming Σ_1 and Σ_2 into two other systems with vanishing disturbances. Then, a delayed controller is utilized to ensure that (31) is attained.

3. Observer-based delayed controller design

The novel observer-based delayed controller is depicted in Fig. 2. Based on the second-order systems (26)-(27), the proposed methodology consists of two main steps:

1. Design a disturbance observer to compensate for disturbances $\sigma_j(t)$, $j = 1,2$. This compensation transforms systems Σ_1 and Σ_2, given in equations (26)-(27), into other ones perturbed by fading disturbances.
2. Using the new systems, a delayed approach is applied to accomplish the control objective (31). To this end, the proportional-retarded delay theory is utilized [59]. Specifically, a proportional-retarded controller ensures that $\boldsymbol{z}(t)$ converges to $\boldsymbol{z}_d(t)$.

To apply the previous methodology, we first split the control inputs $u_j(t)$, $j = 1,2$, as follows

$$u_j(t) = u_{ja}(t) + u_{jb}(t), j = 1,2. \tag{32}$$

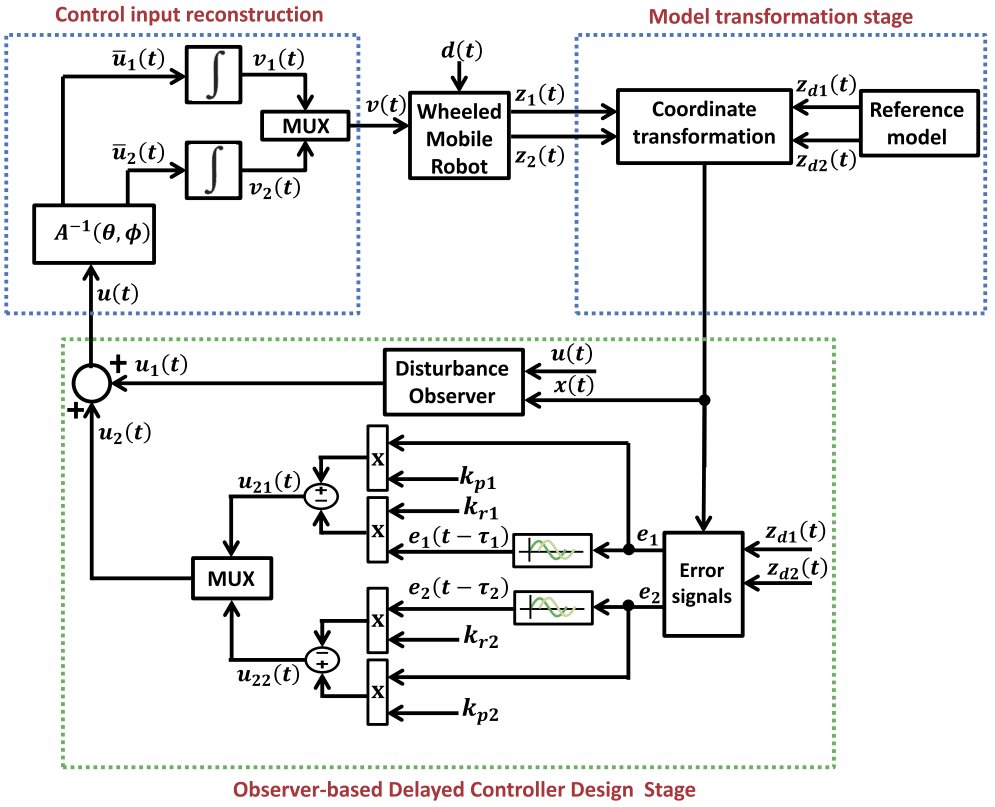

Fig. 2. General diagram of the proposed observer-based delayed controller applied to a WMR.

The controllers $u_{ja}(t)$ will be used to design the disturbance observer, while $u_{jb}(t)$ will be designed by following the proportional-retarded formalism.

Now, we provide the analysis required to design the disturbance observers $u_{ja}(t)$ and the proportional-retarded controllers $u_{jb}(t)$.

3.1. Disturbance-observer design

Based on the asymptotic differentiator proposed in [63], let us consider the following system

$$\frac{d}{dt}\begin{bmatrix}\hat{e}_i\\ \hat{\dot{e}}_i\\ x_{ci}\end{bmatrix}=\begin{bmatrix}k_{oi}\tilde{e}_{1i}+\hat{\dot{e}}_i\\ l_{oi}\text{sign}(\tilde{e}_{1i})\\ u_i\end{bmatrix},\quad i=1,2, \tag{33}$$

with $e_1(t)=x_2(t)-x_{c1}(t)$, $e_2(t)=x_4(t)-x_{c2}(t)$, $\tilde{e}_{1i}(t)=e_i(t)-\hat{e}_i(t)$, $\tilde{e}_{2i}(t)=\dot{e}_i(t)-\hat{\dot{e}}_i(t)$; k_{oi} and l_{oi} are positive constants.

From systems (26)-(27) and (33), note that

$$\begin{aligned}\dot{e}_1(t)&=\dot{x}_2(t)-\dot{x}_{c1}(t)\\&=u_1(t)+\sigma_1(t)-u_1(t)\\&=\sigma_1(t),\\ \dot{e}_2(t)&=\dot{x}_4(t)-\dot{x}_{c2}(t)\\&=u_2(t)+\sigma_2(t)-u_2(t)\\&=\sigma_2(t),\end{aligned}$$

and

$$\begin{aligned}\tilde{e}_{21}(t)&=\dot{e}_1(t)-\hat{\dot{e}}_1(t)\\&=\sigma_1(t)-\hat{\dot{e}}_1(t),\\ \tilde{e}_{22}(t)&=\dot{e}_2(t)-\hat{\dot{e}}_2(t)\end{aligned} \tag{34}$$

$$= \sigma_2(t) - \hat{\tilde{e}}_2(t). \tag{35}$$

From [63], if we select the gains k_{oi} and l_{oi} such that $l_{oi} > \bar{\rho}_i$ and $\left|\dot{\sigma}_i(t)\right| \leq \bar{\rho}_i$, it is ensured that $\tilde{e}_{2i}(t)$, $i = 1, 2$, tend to zero asymptotically, despite any initial condition. Furthermore, the peaking phenomena or chattering is absent in all the signals from (33). Then, from equations (34)-(35), it is clear that $\hat{\tilde{e}}_i(t)$, $i = 1, 2$, tend to $\sigma_i(t)$ asymptotically. Thus, the controllers

$$u_{ia}(t) = -\hat{\tilde{e}}_i(t), \quad i = 1, 2, \tag{36}$$

perform as a disturbance observer.

Then, the disturbance observer (36) is substituted into the equations describing $\dot{x}_2(t)$ and $\dot{x}_4(t)$ from (26)-(27), and we obtain

$$\begin{aligned}
\dot{x}_2(t) &= u_1(t) + \sigma_1(t) \\
&= u_{1a}(t) + u_{1b}(t) + \sigma_1(t) \\
&= (\sigma_1(t) - \hat{\tilde{e}}_1(t)) + u_{1b}(t) \\
&= u_{1b}(t) + \tilde{e}_{21}(t), \\
\dot{x}_4(t) &= u_2(t) + \sigma_2(t) \\
&= u_{2a}(t) + u_{2b}(t) + \sigma_2(t) \\
&= (\sigma_2(t) - \hat{\tilde{e}}_2(t)) + u_{2b}(t) \\
&= u_{2b}(t) + \tilde{e}_{22}(t).
\end{aligned}$$

Then, the second-order systems (26)-(27) are transformed as follows

$$\Sigma_3 \begin{cases} \dot{x}_1(t) = x_2(t), \\ \dot{x}_2(t) = u_{1b}(t) + \tilde{e}_{21}(t), \end{cases} \tag{37}$$

$$\Sigma_4 \begin{cases} \dot{x}_3(t) = x_3(t), \\ \dot{x}_4(t) = u_{2b}(t) + \tilde{e}_{22}(t). \end{cases} \tag{38}$$

At this point, it is essential to note that the original second-order systems Σ_1 and Σ_2 in (26)-(27) are perturbed by the non-vanishing terms $\sigma_i(t)$, $i = 1, 2$. Then, after utilizing the disturbance observer (36), the systems Σ_1 and Σ_2 are transformed into the new second-order systems Σ_3 and Σ_4, as indicated in equations (37)-(38). Systems Σ_3 and Σ_4 are decoupled. Besides, they are perturbed by the vanishing terms $\tilde{e}_{2i}(t)$, $i = 1, 2$, which converge to zero asymptotically. Now, it is left to design the controllers $u_{ib}(t)$, $i = 1, 2$, to accomplish the control objective (31). This design is performed by utilizing the delay theory in the following section.

3.2. Design of the proportional-retarded controller

The previous section demonstrated that, by appropriately selecting the disturbance observer (33), we ensure that the error signals $\tilde{e}_{2i}(t)$, $i = 1, 2$, converge to zero asymptotically, with a high convergence rate. Hence, it may be assumed that the signals $\tilde{e}_{2i}(t)$ values are negligible. Then, the systems Σ_3 and Σ_4 in (37)-(38) can be expressed as the following transfer functions

$$G_1(s) = \frac{x_1(s)}{u_{1b}(s)}, \tag{39}$$

$$G_2(s) = \frac{x_3(s)}{u_{2b}(s)}, \tag{40}$$

where $x_1(s)$, $x_3(s)$, $u_{1b}(s)$, and $u_{2b}(s)$ correspond to the Laplace transform of signals $x_1(t)$, $x_3(t)$, $u_{1b}(t)$, and $u_{2b}(t)$, respectively.

The controllers $u_{ib}(t)$ to be developed utilize the delayed formalism. This is so because, as pointed out in [57], including a delay in the controller aids in attenuating noise or perturbations. Besides, exponential convergence is ensured. Hence, the proposed proportional-retarded controllers $u_{ib}(t)$ have the following mathematical description

$$u_{ib}(s) = k_{pi} - k_{ri} \exp(-s\tau_i), i = 1, 2, \tag{41}$$

with $k_{pi} \in \mathbb{R}^+$ the proportional gain and $k_{ri} \in \mathbb{R}^+$ the delayed gain. Also, $\tau_i \in \mathbb{R}^+$ corresponds to a time delay.

Systems (39)-(40) in closed-loop with (41) yield the following quasi-polynomials

$$p_i(\boldsymbol{k}_i, s) = s^2 + k_{pi} - k_{ri} \exp(-s\tau_i) = 0, i = 1, 2, \tag{42}$$

where $\boldsymbol{k}_i = [k_{pi}, k_{ri}, \tau_i] \in \mathbb{R}^3$.

An appropriate set of gains $\boldsymbol{k}_i$ must be selected to ensure the exponential convergence of (39)-(40) in closed-loop with (41). To this end, reference [64] provides a methodology for choosing the gains $\boldsymbol{k}_i$ by assuming that, given the quasi-polynomials $p_i(\boldsymbol{k}_i, s)$, their roots are continuous functions of the parameter vector $\boldsymbol{k}_i$. Then, let us consider the following definitions.

Definition 1. [64] Assume that all the parameters $\boldsymbol{k}_i$, ensuring that $p_i(\boldsymbol{k}_i, s)$ has at least one purely imaginary root, are contained into the sets Γ_i. Then, the sets Γ_i can be defined as follows

$$\Gamma_i = \{\boldsymbol{k}_i \in K_i : p_i(\boldsymbol{k}_i, s) = 0, s = \pm j\omega, j^2 = -1\}. \tag{43}$$

Definition 2. [64] Let the compact subsets $D_i \subset K_0^i$. Their boundaries $\partial D_i \subset \Gamma_i$, *spectral abscissa* of $p_i(\boldsymbol{k}_i, s)$, corresponding to the regions D_i, are defined as follows

$$\alpha_i^* = \inf\{\alpha_i(\boldsymbol{k}_i) : \boldsymbol{k}_i \in D_i\}, \tag{44}$$

where $\alpha_i : K_0^i \to \mathbb{R}$ such that $\alpha_i(\boldsymbol{k}_i) = \sup\{\mathrm{Re}(s) : p_i(\boldsymbol{k}_i, s) = 0\}$.

Definition 1 shows that the sets Γ_i split K_i into subregions. Each subregion has a constant number of complex roots, each with a positive real part. Specifically, we have that

$$K_i = K_0^i \cup K_1^i \cup K_2^i \cup \cdots, \tag{45}$$

where the sets $K_m^i = \{\boldsymbol{k}_i \in K_i : q_i(\boldsymbol{k}_i, s)\}$ contain precisely m roots with positive real part. These sets K_0^i are termed *stability regions* of the quasi-polynomials (42).

Given the closed-loop systems (39)-(40) with (41), reference [65] provides a temporal relation about the responses $x_1(t)$ and $x_3(t)$, ensuring their exponential convergence as follows.

Lemma 1. *[65] Consider the temporal responses $x_1(t)$ and $x_3(t)$ from systems (39)-(40) in closed-loop with (41). Hence, for each $\sigma_i \in [\alpha_i^*, 0)$, we can find constants L_i and $\bar{\sigma}_i$, $i = 1, 2$, such that*

$$|x_1(t)| \leq L_1 \left|\phi_1\right|_{\tau_1} \exp(\bar{\sigma}_1 t), t \geq 0, \tag{46}$$

$$|x_3(t)| \leq L_2 \left|\phi_2\right|_{\tau_2} \exp(\bar{\sigma}_2 t), t \geq 0, \tag{47}$$

with initial function $\phi \in \mathfrak{C}$ and the Banach space $\mathfrak{C} := C([-\tau_i, 0], \mathbb{R}^n)$ with $\left|\phi_i\right|_{\tau_i} := \max\{\left|\phi_i(\kappa_i)\right| : \kappa_i \in [-\tau_i, 0]\}$.

Next, to determine the performance of responses $x_1(t)$ and $x_3(t)$, we use the spectral abscissa approach [59] to determine the stability regions of the parametric system. This is a geometric method that helps to determine the parametric plane where the gains can be taken for tuning the proportional retarded controller. Besides, this method guarantees a maximum decay rate $\bar{\sigma}^*$ in the closed-loop system responses $x_i(t)$, $i = 1, 2$.

Definition 3. [59] The performance of temporal responses $x_1(t)$ and $x_3(t)$ from the systems (39)-(40) in closed-loop with (41) is settled by $\bar{\sigma}_i = \alpha_i(\boldsymbol{k}_i)$, with $\boldsymbol{k}_i \in D_i$. Moreover, the highest exponential decay occurs if $\alpha_i(\boldsymbol{k}_i^*) = \alpha_i^* = \bar{\sigma}_i^*$, $\boldsymbol{k}_i^* = \left[k_{p_i}^*, k_{r_i}^*, \tau_i^*\right] \in D_i$.

Based on Lemma 1 and Definitions 1-3, the next step is finding a methodology for tuning the gains $\boldsymbol{k}_i$ to guarantee exponential decay. To this end, first consider the parametric curves $\boldsymbol{k}_i$ corresponding to the sets Γ_i, which divide K_i into sub-regions K_m^i, $m \geq 0$. These curves are shown in Fig. 3(a) considering the subsequent conditions:

- If $s = 0$, $p_i(\boldsymbol{k}_i, 0) = 0$, where $k_{pi} = k_{ri}$.
- If $s = j\omega$ and $\omega > 0$, then $p_i(\boldsymbol{k}_i, j\omega) = 0$, where

$$\frac{2m\pi}{\sqrt{k_{pi} - k_{ri}}} \leq \tau_i \leq \frac{(2m+1)\pi}{\sqrt{k_{pi} + k_{ri}}}, i = 1, 2, \tag{48}$$

  with $m = 0, \pm 1, \pm 2, \cdots$, and $0 < k_{ri} < k_{pi}$.

Recall that continuous displacements of the roots of $p_i(\boldsymbol{k}_i, s)$ are generated by continuous variations of its parameters [66]. Then, we can obtain the stability regions $K_0^i \subset K_i$ of systems (39)-(40) in closed-loop with (41), as depicted in Fig. 3(b). Moreover, we can select the compact sets $D_i \subset K_0^i$ from the previous regions K_0^i, as indicated in Fig. 3(c).

With k_{pi} fixed, we can restrain the values of parameters $\boldsymbol{k}_i \in D_i$ to obtain a set ensuring exponential convergence given by $\bar{\sigma}_i$ for coordinates $x_1(t)$ and $x_3(t)$ according to equations (46)-(47). These regions are named σ_i*-stability regions* of $p_i(\boldsymbol{k}_i, s)$. This procedure is given in the following proposition.

Proposition 1. *Let $D_i \subset K_0^i$ and the quasi-polynomial $p_i(\boldsymbol{k}_i, s)$, with $k_{pi} > 0$ fixed. The σ_i-stability regions, where $\bar{\sigma}_i < 0$, are surrounded by the curves produced by the subsequent relations*

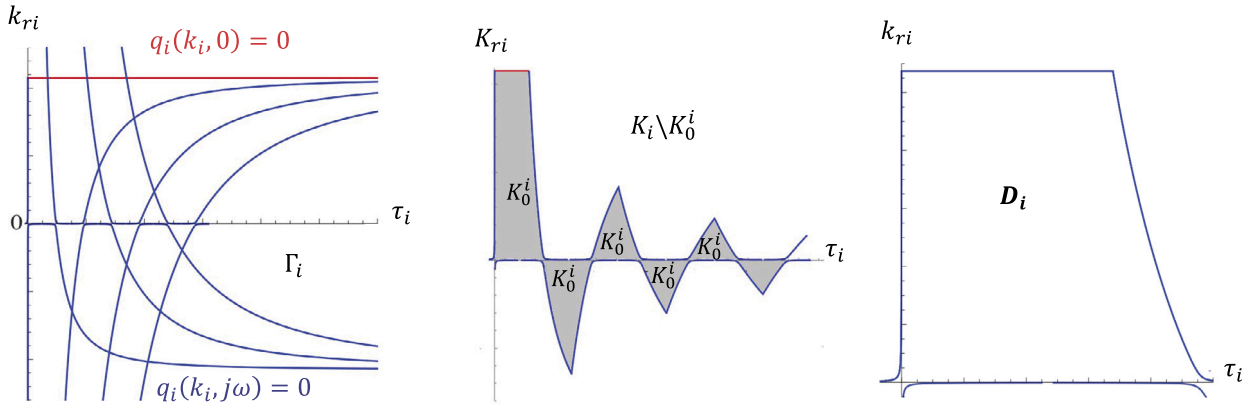

(a) Parametric curves corresponding to Γ_i. **(b)** Stability regions K_0^i. **(c)** Compact set D_i.

Fig. 3. Representation of: (a) parametric curves to define the set Γ_i; (b) stability-regions K_0^i; and (c) compact set D_i in plane $\tau_i - k_{ri}$ with a fixed value of k_{p_i}.

- *If $s = \bar{\sigma}_i$, we have that*

$$k_{ri} = \frac{\bar{\sigma}_i^2 + k_{pi}}{e^{\bar{\sigma}_i \tau_i}}, \quad \tau_i > 0. \tag{49}$$

- *If $s = \bar{\sigma}_i + j\omega$, $j^2 = -1$ and $\omega > 0$, we have that*

$$\tau_i = \frac{1}{\omega} \cot^{-1}\left(\frac{\omega^2 - \bar{\sigma}_i^2 - k_{p_i}}{2\bar{\sigma}_i \omega}\right) + \frac{n\pi}{\omega}, k_{ri} = -\frac{2\bar{\sigma}_i \omega}{\sin(\tau_i \omega)} \exp(\bar{\sigma}_i \tau_i), \ n \in \mathbb{Z}. \tag{50}$$

Proof. Equation (49) is obtained by substituting $s = \bar{\sigma}_i$ at (42) and computing k_{ri}. Also, (50) is obtained by substituting $s = \bar{\sigma}_i + j\omega$ into (42) and obtaining τ_i and k_{ri} from (42). □

Based on the results developed in reference [67], the so-called maximum achievable exponential decay $\bar{\sigma}_i^*$ can be obtained, as stated in the following proposition.

Proposition 2. *Assume the existence of parameters $\boldsymbol{k}_i \in D_i$ such that $p_i(\boldsymbol{k}_i, s)$ has a root $\alpha(\boldsymbol{k}_i)$ with multiplicity three. Then, $\alpha(\boldsymbol{k}_i)$ is dominant, indicating that $\alpha_i^* := \alpha(\boldsymbol{k}_i)$ and $\boldsymbol{k}_i^* := \boldsymbol{k}_i$ represent the highest exponential decay $\bar{\sigma}_i^*$ for signals $x_1(t)$ and $x_3(t)$. Furthermore, given $k_{pi}^* > 0$, the optimal parameters $\bar{\sigma}_i^*$, τ_i^*, and k_{ri}^* are computed as follows*

$$\bar{\sigma}_i^* = -\sqrt{k_{pi}^*}, \ \tau_i^* = \frac{1}{\sqrt{k_{pi}^*}}, \text{ and } k_{ri}^* = -\frac{2\bar{\sigma}_i^*}{\tau_i^*} \exp(\bar{\sigma}_i^* \tau_i^*). \tag{51}$$

Proof. The optimal value $\bar{\sigma}_i^*$ is obtained by utilizing the results presented in [67]. Besides, the polynomials (42) have a root with three multiplicities at $\bar{\sigma}_i$ when $p_i(k_i, \bar{\sigma}_i) = 0$, $\frac{\partial}{\partial \bar{\sigma}_i} p_i(k_i, \bar{\sigma}_i) = 0$, and $\frac{\partial^2}{\partial \bar{\sigma}_i^2} p_i(k_i, \bar{\sigma}_i) = 0$, i.e.

$$0 = \bar{\sigma}_i^2 + k_{pi} - k_{ri} \exp(\bar{\sigma}_i \tau_i), 0 = 2\bar{\sigma}_i + \tau_i k_{ri} \exp(\bar{\sigma}_i \tau_i), 0 = 2 - \tau_i^2 k_{ri} \exp(\bar{\sigma}_i \tau_i). \tag{52}$$

Then, expressions (51) can be computed by solving (52) for $\bar{\sigma}_i$, τ_i, and k_{ri}. □

Finally, Proposition 2 can be rewritten in an alternative way that simplifies the computation of the controller gains $\boldsymbol{k}_i$. This modification is given below.

Proposition 3. *Let the highest exponential decay $\bar{\sigma}_i^* < 0$. Then, the parameters $\boldsymbol{k}_i^* = \left[k_{pi}^*, k_{ri}^*, \tau_i^*\right] \in D_i \subset K_0^i$ that yield $\bar{\sigma}_i^*$ for signals $x_1(t)$ and $x_3(t)$ are given by*

$$k_{pi}^* = \left(\bar{\sigma}_i^*\right)^2, \tau_i^* = -\frac{1}{\bar{\sigma}_i^*}, k_{ri}^* = -\frac{2\bar{\sigma}_i^*}{\tau_i^*} \exp(\bar{\sigma}_i^* \tau_i^*). \tag{53}$$

Proof. The equations for the optimal gains are obtained from Proposition 3 by expressing (51) as (53). □

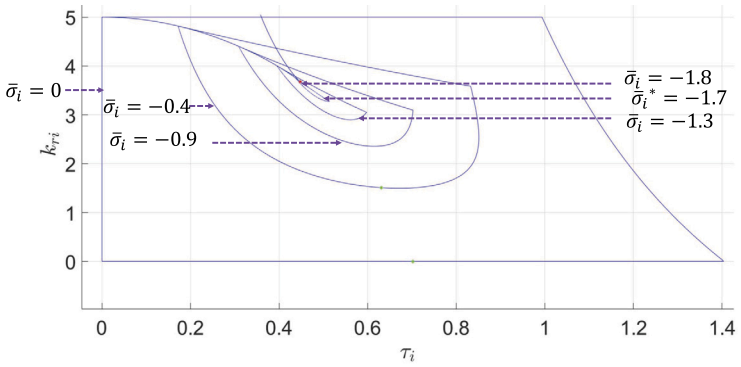

Fig. 4. Graphic of the σ-stability regions of $p_i(\boldsymbol{k}_i, s)$ when $k_{pi} = 5$.

Application of Proposition 1 allows depicting the σ_i-stability regions for a given compact set D_i. In Fig. 4, the σ_i-stability regions of the quasi-polynomial $p_i(\boldsymbol{k}_i, s)$ given in (42) are depicted for $k_{pi} = 5$. Here, it can be verified that the optimal value is obtained at $\bar{\sigma}_i^* = -1.7$, which corresponds to $k_{ri} = 3.79$. Hence, we observe that the σ_i-stability regions converge to the optimal parameters $\boldsymbol{k}_i^* = [k_{pi}^*, k_{ri}^*, \tau_i^*] = [5, 3.79, 0.47]$.

In conclusion, based on Lemma 1, it is ensured that signals $x_1(t)$ and $x_3(t)$ converge to zero exponentially when the controllers (41) are applied to the systems (39)-(40). Recall that

$$\begin{aligned} x_1(t) &= \tilde{z}_1(t) \\ &= z_1(t) - z_{d1}(t), \end{aligned} \tag{54}$$

$$\begin{aligned} x_3(t) &= \tilde{z}_2(t) \\ &= z_2(t) - z_{d2}(t). \end{aligned} \tag{55}$$

Therefore, convergence of $x_1(t)$ and $x_3(t)$ to zero ensures that the control objective (31) is attained. Furthermore, because signals $\tilde{e}_{2i}(t)$ converge to zero asymptotically, it is concluded that the convergence of $\boldsymbol{z}(t)$ to $\boldsymbol{z}_d(t)$ is asymptotic.

The previous analysis allows the design of $u_1(t)$ and $u_2(t)$. However, the WMR's signals $v_1(t)$ and $v_2(t)$ are the ones required to control the vehicle. Then, we can recover these control inputs as follows

$$\boldsymbol{v}(t) = \begin{bmatrix} v_1(t) \\ v_2(t) \end{bmatrix} = \begin{bmatrix} \int_0^t \bar{u}_1(\tau) d\tau \\ \int_0^t \bar{u}_2(\tau) d\tau \end{bmatrix}, \tag{56}$$

where

$$\bar{\boldsymbol{u}}(t) = A(\theta, \phi)^{-1} \boldsymbol{u}(t),$$

$$\boldsymbol{u}(t) = \begin{bmatrix} u_1(t) & u_2(t) \end{bmatrix}^T = \begin{bmatrix} u_{1a}(t) + u_{1b}(t) & u_{2a}(t) + u_{2b}(t) \end{bmatrix}^T.$$

Now, we have developed all the tools needed to design the novel controller. We summarize these results as follows.

Theorem 1. *Let the WMR's kinematic model (1). The control objective (31) is ensured by using the controller*

$$\boldsymbol{u}(t) = \begin{bmatrix} u_1(t) & u_2(t) \end{bmatrix}^T = \begin{bmatrix} u_{1a}(t) + u_{1b}(t) & u_{2a}(t) + u_{2b}(t) \end{bmatrix}^T, \tag{57}$$

where

$$u_{ia}(t) = -\hat{e}_i(t), i = 1, 2, \tag{58}$$

$$u_{ib}(s) = k_{pi} - k_{ri} \exp(-s\tau_i), \tag{59}$$

with

$$\frac{d}{dt} \begin{bmatrix} \hat{e}_i \\ \hat{\dot{e}}_i \\ x_{ci} \end{bmatrix} = \begin{bmatrix} k_{oi} \tilde{e}_{1i} + \hat{\dot{e}}_i \\ l_{oi} \text{sign}(\tilde{e}_{1i}) \\ u_i \end{bmatrix}, \quad i = 1, 2; \tag{60}$$

and $e_1(t) = x_2(t) - x_{c1}(t)$, $e_2(t) = x_4(t) - x_{c2}(t)$, $\tilde{e}_{1i}(t) = e_i(t) - \hat{e}_i(t)$, $\tilde{e}_{2i}(t) = \dot{e}_i(t) - \hat{\dot{e}}_i(t)$, $\boldsymbol{z}(t) = [z_1(t), z_2(t)]^T$, $\boldsymbol{z}_d(t) = [z_{d1}(t), z_{d2}(t)]^T$, $\tilde{\boldsymbol{z}}(t) = [\tilde{z}_1(t), \tilde{z}_2(t)]^T = \boldsymbol{z}(t) - \boldsymbol{z}_d(t)$, $x_1(t) = \tilde{z}_1(t)$, $x_2(t) = \dot{\tilde{z}}_1(t)$, $x_3(t) = \tilde{z}_2(t)$, $x_4(t) = \dot{\tilde{z}}_2(t)$; *also,* k_{oi}, l_{oi}, k_{pi}, k_{ri}, *and* τ_i *are positive constants.*

Proof. Given the WMR's kinematic model (1), we can utilize definitions (8) and (9) to obtain the error equation (21). Now, we employ the new states (22)-(25) to transform the previous error equation into the two decoupled second-order systems (26)-(27). Now, we split the control inputs as indicated in (32). By utilizing the disturbance observer (33), the controllers $u_{ia}(t)$ are designed according to (36), which yields (37)-(38). Now, the control inputs $u_{ib}(t)$ are designed as a proportional-retarded controller, as indicated in equation (41). Then, according to Lemma 1, it is ensured that $x_1(t)$ and $x_3(t)$ converge to zero, which implies that the control objective (31) is accomplished. Finally, $v_1(t)$ and $v_2(t)$ are recovered by utilizing (56), which completes the proof. □

Remark 2. Note that Theorem 1 ensures that $x_i(t)$, $i = 1,2,3,4$ converge to zero asymptotically. This fact implies that $\tilde{\boldsymbol{z}}(t)$ and $\dot{\tilde{\boldsymbol{z}}}(t)$ also converge to zero asymptotically. Then, it is clear that $\lim_{t\to\infty}\left[A(\theta,\phi)\boldsymbol{v} - A(\theta_d,\phi_d)\boldsymbol{v}_d\right] = 0$ for every $\theta(t)$, $\phi(t)$, $\theta_d(t)$, $\phi_d(t)$, $\boldsymbol{v}(t)$ and $\boldsymbol{v}_d(t)$. Therefore, it is concluded that $\lim_{t\to\infty}\theta(t) = \theta_d(t)$, $\lim_{t\to\infty}\phi(t) = \phi_d(t)$, and $\lim_{t\to\infty}\boldsymbol{v}(t) = \boldsymbol{v}_d(t)$. Now, from the convergence of $\tilde{\boldsymbol{z}}(t)$ to zero and equations (8)-(9), we obtain $\lim_{t\to\infty}\left[x - x_d + l\left[c_\theta - c_{\theta_d}\right] + \delta\left[c_{\theta+\phi} - c_{\theta_d+\phi_d}\right]\right] = 0$ and $\lim_{t\to\infty}\left[y - y_d + l\left[s_\theta - s_{\theta_d}\right] + \delta\left[s_{\theta+\phi} - s_{\theta_d+\phi_d}\right]\right] = 0$, which implies that $\lim_{t\to\infty}x(t) = x_d(t)$ and $\lim_{t\to\infty}y(t) = y_d(t)$. Hence, it can be inferred that the asymptotic convergence of $x_i(t)$, $i = 1,2,3,4$ to zero implies that $\boldsymbol{q}(t)$ converges to $\boldsymbol{q}_d(t)$ asymptotically.

The previous development ensures that (31) is realized using the novel proposal. For simplicity, the novel observer-based proportional-retarded controller (57)-(60) will be termed the OPR controller. Note that an advantage of the proportional retarded controllers $u_{ib}(s)$ in (59) is that no velocity measurements are required. Besides, using the disturbance observer implies that the disturbances affecting the closed-loop system can be compensated, augmenting the controller's robustness. Hence, it may be expected that the performance of the WMR, when controlled with the OPR methodology, will be robust against disturbances. In the following section, we will assess the OPR's performance experimentally. This novel scheme will be compared against other robust control techniques from the literature.

4. Experimental validation of the OPR controller

This section presents the experimental results that validate the performance of the proposed OPR controller. To this end, we employed a scaled experimental platform. Also, to demonstrate the novel controller's outstanding performance, different robust controls from the literature were utilized.

4.1. Experimental platform

The novel OPR controller was assessed experimentally by using the experimental platform Autominy [68]. The experimental platform utilized in the following experiments is depicted in Fig. 5. The Autominy vehicle is a 1:10 autonomous model car. The control algorithms are processed by an Intel NUC CPU, allowing the car to perform autonomously. The steering movement is achieved through a servo motor, while a direct current motor allows the vehicle's longitudinal movement. This system has a LiDar (Light Detection and Ranging) sensor and an Intel Real Sense D435 camera.

As indicated in Fig. 5, one computer works as the base station to perform the experiments. In this computer, the control algorithms are programmed using Matlab-Simulink. Then, the control signals are sent to the vehicle wirelessly. To this end, the Robotic Operating System [69] is utilized. The Autominy runs Ubuntu 18.04 [70] with ROS Noetic Ninjemys. The communication between the base station and the Autominy is performed via topics. Finally, a stationary multi-camera system obtains the vehicle position and orientation.

Remark 3. Note that the experimental platform is always affected by different types of disturbances. For instance, wireless communication provides noisy measurements and may generate communication delays. Besides, the vehicle operates on soft mats that affect its movement. The multi-camera system also introduces some measurement errors. Hence, a good closed-loop performance implies that the controller is robust against these different disturbance sources.

4.2. Controller used for comparison

The following experiments assess the performance of the novel OPR controller. To this end, we used four different robust controllers. Specifically, an observer-based H_∞ controller [71], a feedback controller [21], a proportional integral derivative (PID) methodology [72], and a backstepping-sliding modes controller [45]. For simplicity, the observer-based H_∞, feedback, PID, and backstepping-sliding modes controllers are termed HI, FC, PID, and FT controllers, respectively.

The HI controller is mathematically described as follows [71]

$$u_i(t) = u_{HI,1i}(t) + u_{HI,2i}(t), \quad i = 1,2, \tag{61}$$

where

$$u_{HI,1i}(t) = -\hat{\hat{e}}_i(t),$$
$$u_{HI,21}(t) = -\frac{1}{2}\left[\beta_2 x_1(t) + \beta_3 x_2(t)\right],$$

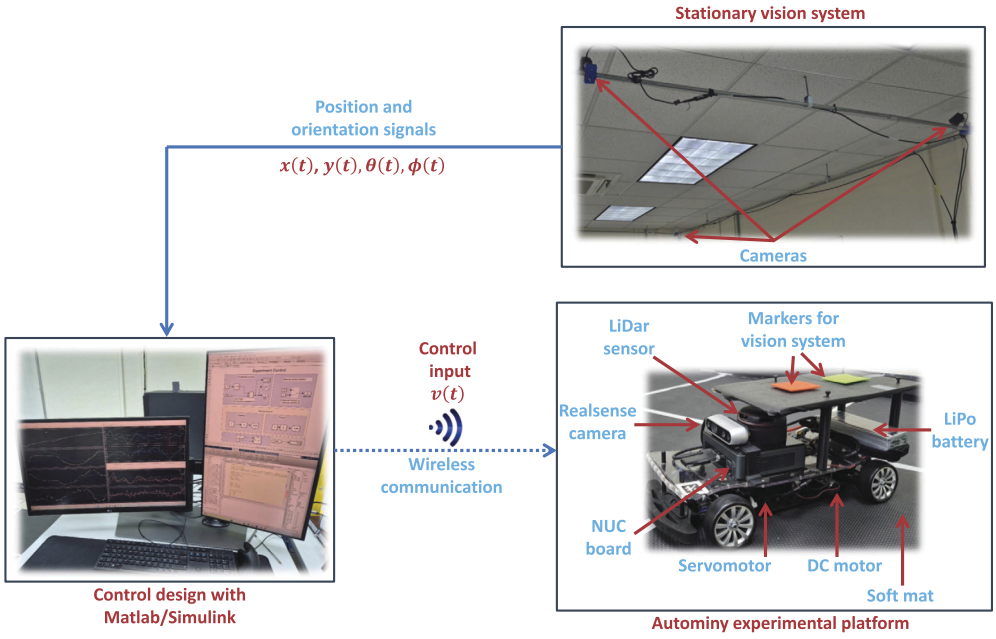

Fig. 5. Autominy experimental platform used in the trajectory-tracking tests.

$$u_{HI,22}(t) = -\frac{1}{2}\left[\beta_5 x_3(t) + \beta_6 x_4(t)\right],$$

with β_2, β_3, β_5 and β_6 some positive constants.

To apply the feedback controller FC, it is required to use the following kinematic model in chained form [21]

$$\begin{aligned} \dot{\zeta}_1(t) &= u_1(t), \\ \dot{\zeta}_2(t) &= u_2(t), \\ \dot{\zeta}_3(t) &= \zeta_2(t)u_1(t), \\ \dot{\zeta}_4(t) &= \zeta_3(t)u_1(t), \end{aligned} \tag{62}$$

with $\zeta_1(t) = x(t)$, $\zeta_2(t) = t_\phi/(lc_\theta^3)$, $\zeta_3(t) = t_\theta$, and $\zeta_4(t) = y(t)$. Then, the FC scheme is described by [21]

$$\begin{aligned} v_1(t) &= \frac{u_{FC,1}(t)}{c_\theta}, \\ v_2(t) &= -\frac{3s_\theta s_\phi^2}{lc_\theta^2}u_{FC,1}(t) + lc_\theta^3 c_\phi^2 u_{FC,2}(t), \end{aligned} \tag{63}$$

where

$$\begin{aligned} u_{FC,1}(t) &= \psi_1(t), \\ u_{FC,2}(t) &= \frac{r_2(t) - \zeta_3(t)r_1(t) - 3\zeta_2(t)\psi_1(t)\psi_2(t)}{\psi_1^2(t)}, \\ \dot{\psi}_1(t) &= \psi_2(t), \\ \dot{\psi}_2(t) &= r_1(t), \\ r_1(t) &= \ddot{\zeta}_{d1} + k_{a1}\left[\ddot{\zeta}_{d1}(t) - \ddot{\zeta}_1(t)\right] + k_{v1}\left[\dot{\zeta}_{d1}(t) - \dot{\zeta}_1(t)\right] + k_{FC,p1}\left[\zeta_{d1}(t) - \zeta_1(t)\right], \\ r_2(t) &= \ddot{\zeta}_{d4} + k_{a2}\left[\ddot{\zeta}_{d4}(t) - \ddot{\zeta}_4(t)\right] + k_{v2}\left[\dot{\zeta}_{d4}(t) - \dot{\zeta}_4(t)\right] + k_{FC,p2}\left[\zeta_{d4}(t) - \zeta_4(t)\right], \end{aligned} \tag{64}$$

ζ_{dj}, $j = 1, ..., 4$ are the corresponding reference signals from the chained model (62), and k_{ai}, k_{vi}, $k_{FC,pi}$, $i = 1, 2$, are positive constants.

The description of the PID controller is given by

$$\begin{aligned} u_i(t) &= u_{PID,ia}(t) + u_{PID,ib}(t),\ i = 1, 2, \\ u_{PID,ia}(t) &= -\hat{e}_i(t),\ i = 1, 2, \\ u_{PID,1b}(t) &= -k_{PID,p1}x_1(t) - k_{PID,d1}x_2(t) - k_{PID,i1}\varsigma_1(t), \\ u_{PID,2b}(t) &= -k_{PID,p2}x_3(t) - k_{PID,d2}x_4(t) - k_{PID,i2}\varsigma_2(t), \end{aligned} \tag{65}$$

where $k_{PID,pj}$, $k_{PID,dj}$, $k_{PID,ij}$, $j = 1, 2$, are positive constants with $k_{PID,dj}$ sufficiently large and $k_{PID,ij} < 1/k_{PID,dj}$.

Finally, the mathematical description of the FT controller is as follows [45]

$$\begin{aligned}
&u_i(t) = u_{di}(t) - \tilde{u}_i(t),\ i = 1,2,\\
&\tilde{u}_1(t) = -k_4 \left|\eta_4(t)\right|^{1/2} \operatorname{sign}(\eta_4(t)),\\
&\tilde{u}_2(t) = \left[(k_1^2 - 1)\eta_2(t) - (k_1 + k_2)(-k_1^2\eta_1 + k_1\xi_1 + \eta_3)\right] u_{d1}(t) - k_3\xi_2(t)u_{d1}(t),\\
&\xi_1(t) = \eta_2(t) + k_1\eta_1(t),\\
&\xi_2(t) = \eta_3(t) - (k_1^2 - 1)\eta_1(t) + (k_1 + k_2)\xi_1(t),
\end{aligned} \tag{66}$$

where $\tilde{\zeta}_i(t) = \zeta_{di}(t) - \zeta_i(t)$, $i = 1,2,3,4$, $\eta_1(t) = \tilde{\zeta}_4(t) + (\tilde{\zeta}_3(t) - \zeta_{d3}(t))\tilde{\zeta}_1(t)$, $\eta_2(t) = \tilde{\zeta}_3(t) + (\tilde{\zeta}_2(t) - \zeta_{d2}(t))\tilde{\zeta}_1(t)$, $\eta_3(t) = \tilde{\zeta}_2(t)$, $\eta_4(t) = \tilde{\zeta}_1(t)$, and $u_{di}(t)$ are the desired reference inputs corresponding to the chained model (62). Moreover, gains k_i, $i = 1,2,3,4$, are positive.

In the following Section, the experiments concerning the HI [71], FC [21], PID [72], FT [45], and OPR controllers are presented. It is essential to note that not all the controllers taken from the literature present experimental results. Specifically, references [21] and [45] have numerical simulations only, while [71] and [72] have numerical simulations and experiments. Besides, it is worth mentioning that, in references [21], [45], [71], and [72], the control design is presented, but a methodology for tuning the controller's gains is absent. Then, the selection of the gains for each controller took into account each controller's best transient and steady-state performance; also, the selection of the gains aimed to make each controller reach the desired control inputs in about five seconds; furthermore, it was verified that the gain's selection avoids actuator saturation. The previous considerations verified that the controller [21] yields high gains if the roots from $p_i(\lambda) = \lambda^3 + k_{ai}\lambda^2 + k_{vi}\lambda + k_{FC,pi}$, $i = 1,2$, are selected at $\lambda < -1$; hence, we selected all the roots at $\lambda = -0.6$. For reference [45], it was verified that k_4 is directly related to $x(t)$; then, this gain was selected to make $x(t)$ converge to $x_d(t)$ as fast as possible while ensuring that $v_1(t)$ converges to $v_{d1}(t)$ in about five seconds; furthermore, k_1 and k_2 were selected to avoid oscillations in $\theta(t)$ while improving the tracking performance in $y(t)$. References [71] and [72] have a similar structure as that reported in this manuscript; then, the corresponding gains were selected to make $v_1(t)$ converge to $v_{d1}(t)$ in about five seconds while reducing the tracking errors in coordinates $x(t)$ and $y(t)$; also, the corresponding selection was made to avoid input saturation and oscillations in $\theta(t)$. The previous considerations yielded the following set of gains:

- HI: $\beta_2 = 12$, $\beta_3 = 8$, $\beta_5 = 12$, $\beta_6 = 8$, $k_{o1} = 100$, $l_{o1} = 1$, $k_{o2} = 100$, $l_{o2} = 1$, $\delta = 1$.
- FC: $k_{FC,p1} = 0.216$, $k_{FC,p2} = 0.216$, $k_{v1} = 1.08$, $k_{v2} = 1.08$, $k_{a1} = 1.8$, $k_{a2} = 1.8$.
- PID: $k_{PID,p1} = 12$, $k_{PID,p2} = 12$, $k_{PID,d1} = 8$, $k_{PID,d2} = 8$, $k_{PID,i1} = 0.05$, $k_{PID,i2} = 0.05$, $k_{o1} = 100$, $l_{o1} = 1$, $k_{o2} = 100$, $l_{o2} = 1$, $\delta = 1$.
- FT: $k_1 = 3$, $k_2 = 6$, $k_3 = 4$, $k_4 = 0.3$.
- OPR: $k_{p1} = 5$, $k_{r1} = 4.54$, $k_{p2} = 4.5$, $k_{r2} = 3.99$, $\tau_1 = 0.24$, $\tau_2 = 0.24$, $\delta = 1$.

All the experiments utilized Matlab-Simulink with a sampling time of $10\,[ms]$ and solver Ode5 DormanPrince. The position and orientation estimation was performed with a vision algorithm running in Matlab-Simulink 2022b, while the control algorithms were performed using Matlab 2018b.

By following the same lines described in [72], the reference signal was designed according to the following equations

$$\begin{aligned}
x_d(t) &= \frac{3.5776}{13}t + 0.625,\\
y_d(t) &= \frac{2.3876}{13}t + 0.625,\\
\theta_d(t) &= \operatorname{atan2}\left\{\frac{\dot{y}(t)}{v_{d1}(t)}, \frac{\dot{x}_d(t)}{v_{d1}(t)}\right\},\\
\phi_d(t) &= \operatorname{atan2}\left\{l\left[\ddot{y}_d(t)\dot{x}_d(t) - \ddot{x}_d(t)\dot{y}_d(t)\right], v_{d1}^3(t)\right\},\\
v_{d1}(t) &= \sqrt{\dot{x}_d^2 + \dot{y}_d^2},\\
v_{d2}(t) &= l v_{d1}(t)\frac{\kappa_1 - 3\kappa_2}{v_{d1}^6(t) + \kappa_3},\\
\kappa_1(t) &= \left[\ddot{y}_d(t)\dot{x}_d(t) - \ddot{x}_d(t)\dot{y}_d(t)\right] v_{d1}^2(t),\\
\kappa_2(t) &= \left[\ddot{x}_d(t)\dot{x}_d(t) + \ddot{y}_d(t)\dot{y}_d(t)\right]\left[\ddot{y}_d(t)\dot{x}_d(t) - \ddot{x}_d(t)\dot{y}_d(t)\right],\\
\kappa_3(t) &= l^2\left[\ddot{y}_d(t)\dot{x}_d(t) - \ddot{x}_d\dot{y}_d(t)\right]^2.
\end{aligned}$$

4.3. Experimental results

The experimental results when applying the HI, FC, PID, FT, and OPR controllers are depicted in the following. Besides, a video with the following experiments can be consulted in [73]. Fig. 6 shows the tracking errors $\tilde{x}(t) = x(t) - x_d(t)$, $\tilde{y}(t) = y(t) - y_d(t)$, $\tilde{\theta}(t) = \theta(t) - \theta_d(t)$, and $\tilde{\phi}(t) = \phi(t) - \phi_d(t)$. For the first tracking error, $\tilde{x}(t)$, we observe that the OPR controller has the fastest response and makes the error signal converge to zero in about three seconds. The HI, PID, and FT controllers converge to a neighborhood of zero in six seconds, while the FC controller lasts seven seconds. However, only the FC, PID, and FT controllers remain close to the

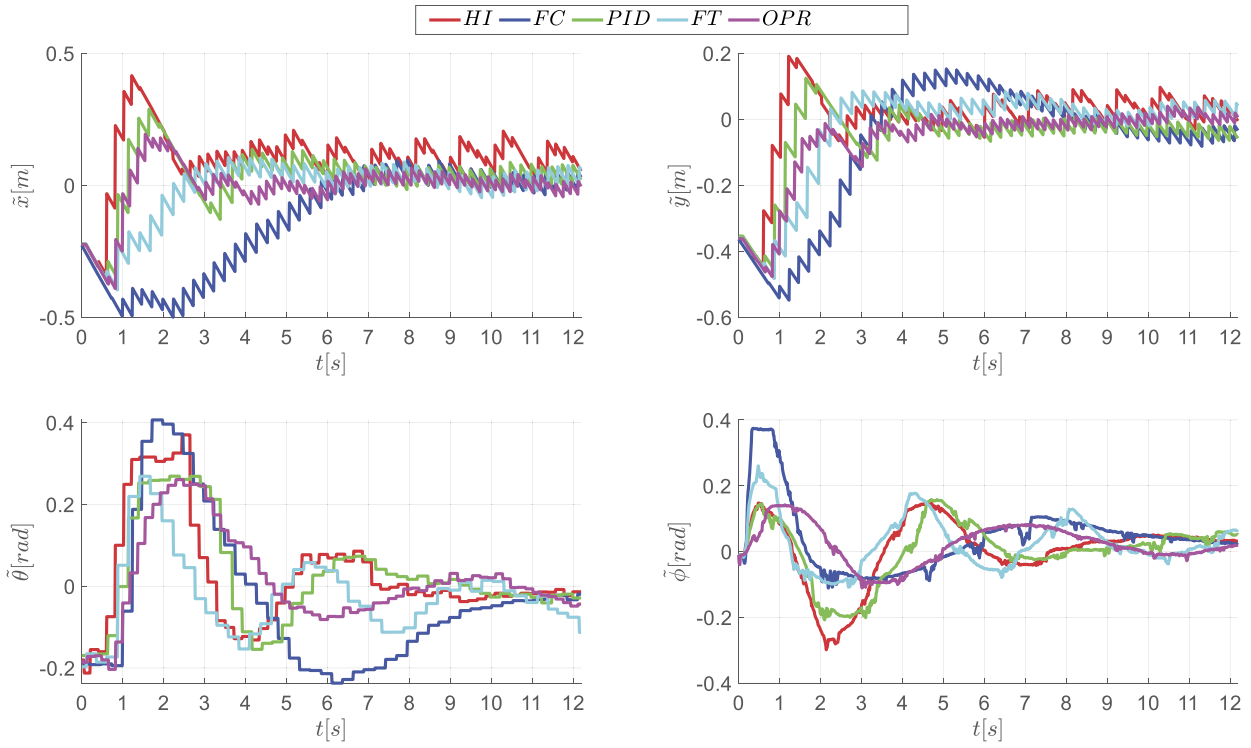

Fig. 6. Temporal response of the tracking errors $\tilde{x}(t) = x(t) - x_d(t)$, $\tilde{y}(t) = y(t) - y_d(t)$, $\tilde{\theta}(t) = \theta(t) - \theta_d(t)$, and $\tilde{\phi}(t) = \phi(t) - \phi_d(t)$ when utilizing the HI, FC, PID, FT, and OPR controllers in the experimental platform Autominy.

origin, while the HI control scheme exhibits oscillations around zero and overshoot. Moreover, note that the OPR controller is the only one maintaining a slight variation around zero. Hence, the OPR controller exhibits the best performance for this first coordinate.

For the second error signal, $\tilde{y}(t)$, the HI controller quickly converges to the origin. However, as in the previous case, it exhibits oscillations and overshoot. The OPR controller converges to a neighborhood of zero in about three seconds; besides, it remains close to zero all the remaining time. The FT and PID controllers also converge to a neighborhood of zero as fast as the OPR controller; however, these schemes exhibit a tracking error more significant than that obtained with the OPR methodology. The worst efficiency is attained with the FC control scheme, which shows an overshoot and does not seem to converge to zero. Then, these results demonstrate that, for the second coordinate, the OPR controller remains to have the best performance.

All the controllers exhibit similar performance for orientation error $\tilde{\theta}(t)$. However, the most considerable overshoot is attained using the FC methodology, pursued by the HI, FT, PID, and OPR controllers. Based on the overshoot feature, it can be concluded that the OPR controller outperforms the other control methodologies.

Finally, for the steering angle error $\tilde{\phi}(t)$, as in the previous cases, the most considerable overshoot is attained when applying the FC scheme, pursued by the FT, HI, PID, and OPR controllers. Although all the controllers remain in the vicinity of the origin after a while, the OPR methodology remains closer to the origin. Hence, the proposed controller exhibits the best performance.

In Fig. 6, some significant fluctuations appear for coordinates $x(t)$ and $y(t)$. This effect is generated by the different disturbances mentioned in Remark 3, which affect the closed-loop system. The noisy measurements acquired through the wireless communication system are the main factor that generates such fluctuations. It can be verified through numerical simulations that, in the free-noise case, the resulting signals do not exhibit this behavior. However, when noise is introduced to the measured position and orientation signals, it produces the behavior visualized in Fig. 6.

Fig. 7 depicts $v_1(t)$ and $v_2(t)$. Also, the corresponding reference inputs $v_{d1}(t)$ and $v_{d2}(t)$ are shown. Besides, for the first control input, the PID and the HI controllers are the ones that demand the largest input values. The OPR and FT controllers have a similar performance and converge to the desired reference $v_{d1}(t)$; however, the FT methodology exhibits some oscillations around the reference input. Moreover, the FC methodology requests the lowest input values, converging to the desired reference in about seven seconds.

For $v_2(t)$, all the controllers track $v_{d2}(t)$. Nevertheless, the FC scheme requires the largest control inputs, followed by the FT, HI, PID, and OPR controllers. Thus, the novel OPR controller requires input signals with low demands.

To obtain a more precise panorama of the trajectory the Autominy vehicle follows, we provide the WMR's time evolution in plane **xy** in Fig. 8. Note that the slowest convergence is attained using the FC scheme. Initially, the HI, PID, FT, and OPR controllers exhibit a similar behavior. Nevertheless, note that, after two seconds, the OPR methodology remains closer to the desired reference signal when compared to the other control schemes. Also, the HI, FC, and PID controllers exhibit a remaining tracking error, while the

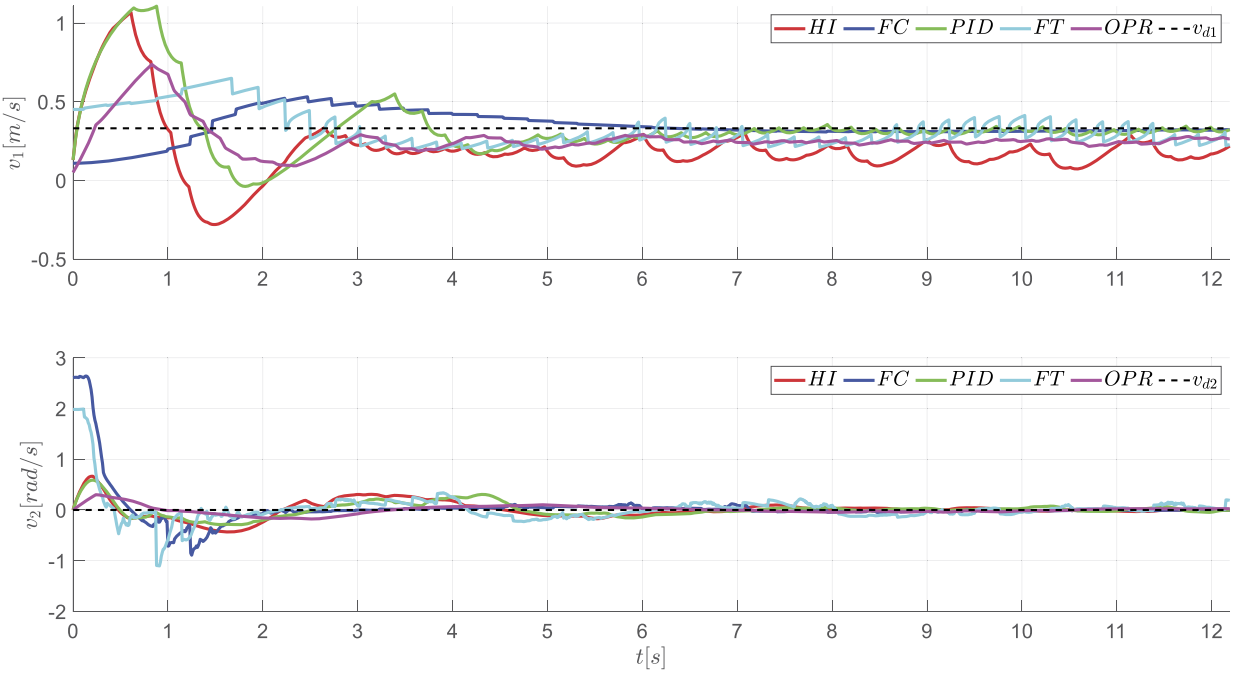

Fig. 7. Temporal response of the control inputs $v_1(t)$, $v_2(t)$ and their corresponding desired control inputs $v_{d1}(t)$ and $v_{d2}(t)$ when using the HI, FC, PID, FT, and OPR controllers in the experimental platform Autominy.

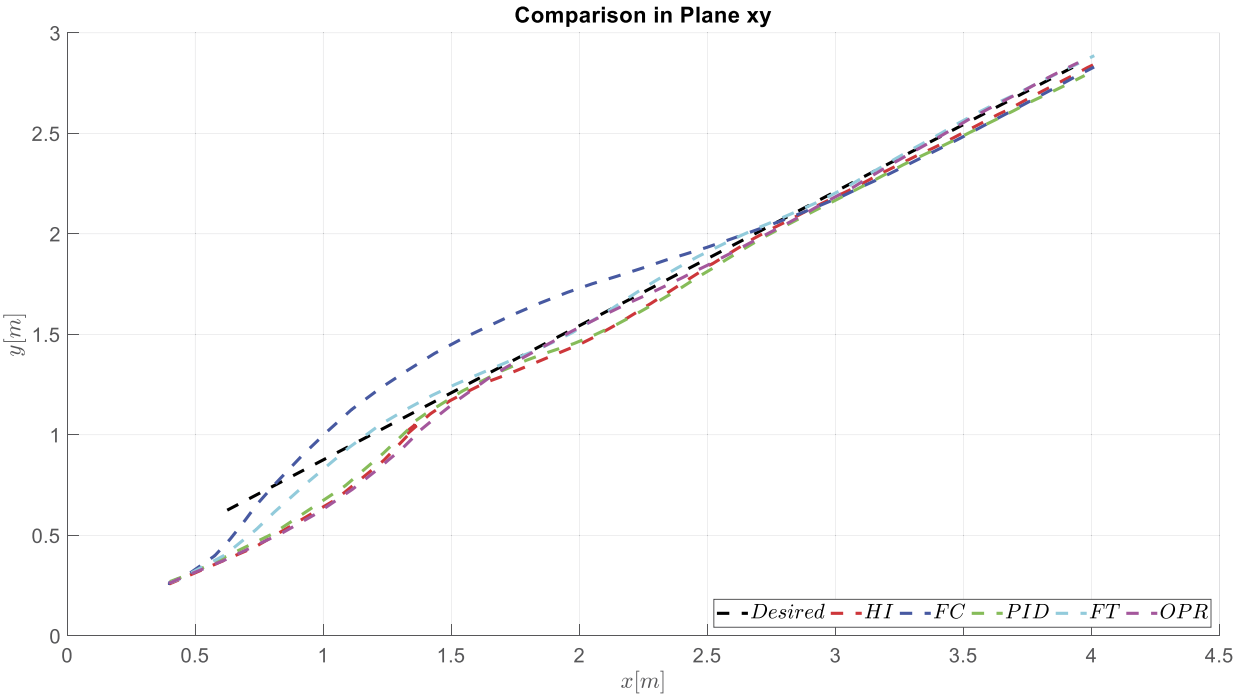

Fig. 8. Trajectory-tracking response in plane **xy** when applying the HI, FC, PID, FT and OPR controllers to the experimental platform Autominy.

FT and OPR controllers are the ones that keep closer to the reference signal. Hence, it may be concluded that the new OPR control scheme outperforms the other methodologies.

Now, we complement the data provided by Figs. 6-8 with quantitative data. Specifically, we computed the following performance indexes:

Table 1
Experimental results for the performance indexes IAE, $ITSE$ and $ITAE$ when using the HI, FC, PID, FT, and OPR controllers with the experimental platform Autominy.

	IAE				$ITSE$				$ITAE$			
	e_x	e_y	e_θ	e_ϕ	e_x	e_y	e_θ	e_ϕ	e_x	e_y	e_θ	e_ϕ
HI	163.5	**78.7**	108.4	88.1	114.8	20.1	47.7	36.8	844.0	287.7	351.0	378.9
FC	199.3	170.3	179.9	95.5	143.6	86.1	146.9	33.3	594.1	523.2	815.9	415.2
PID	102.5	82.5	108.4	78.3	33.8	19.1	48.5	31.9	392.3	253.0	381.1	340.7
FT	88.8	103.8	**94.4**	74.7	23.6	29.7	**36.4**	28.0	294.8	289.9	395.7	332.3
OPR	**68.1**	81.8	96.8	**61.7**	**13.8**	**17.9**	37.5	**17.6**	**195.3**	**175.8**	**342.7**	**273.9**

Table 2
Experimental results for the performance indexes RMS and ISV when using the HI, FC, PID, FT, and OPR controllers with the experimental platform Autominy.

	RMS				ISV
	e_x	e_y	e_θ	e_ϕ	
HI	5.42	**3.90**	4.65	3.44	**117.6**
FC	8.16	7.29	6.32	3.90	172.9
PID	4.04	4.34	4.34	3.06	343.47
FT	3.94	5.17	**3.54**	2.87	238.11
OPR	**3.45**	4.64	3.86	**2.22**	263.73

- The integral of the absolute value of tracking error (IAE). This performance index is computed by $IAE = \int_0^T |\epsilon(t)|\, dt$.
- Integral of time multiplied by the square error (ITSE). We have that $ITSE = \int_0^T t\epsilon^2(t)dt$.
- Integral of the time multiplied by the absolute value of the tracking error (ITAE). We compute $ITAE = \int_0^T t\,|\epsilon(t)|\, dt$.
- The root mean squared error (RMS). We have that $RMS = \sqrt{\frac{1}{T}\int_0^T \epsilon^2(t)dt}$.
- Integral of the input's square value (ISV). This performance index is computed by $ISV = \int_0^T u^2(t)dt$,

where $u(t)$ denotes the corresponding control input, $\epsilon(t)$ a given tracking error signal, and T the experimental time.

The IAE, ITSE, and ITAE values are given in Table 1, while the RMS and ISV values are given in Table 2. In Table 1, as expected, we observe that almost all the lowest values are obtained with the novel OPR controller. For the ITAE performance index, the OPR's values corresponding to coordinates $y(t)$ and $\phi(t)$ are close to the minimum ones. The same happens with the ITSE performance index, while all the minimum ITAE values are obtained with the proposed control scheme. The information from Table 2 shows a similar behavior with the OPR controller. Finally, the HI control scheme requests the minimum input values, pursued by the FC, FT, OPR, and PID methodologies.

The previous data corroborates the information provided by Figs. 6-8, indicating that the best performance is achieved with the new OPR methodology. Also, the information from Table 1 confirms that the proposed OPR control scheme has the lowest error deviations and less time is required to diminish the tracking errors.

Finally, note that a remarkable behavior is obtained despite the inherent disturbances in the experimental platform. Recall from Remark 3 that the experimental platform is always affected by disturbances such as kinematic perturbations introduced by the soft mats used as flooring material, measurement noise generated by the wireless communication, and measurement errors generated by the multicamera system. However, despite these effects, the closed-loop efficiency is remarkable when utilizing the OPR controller. This behavior indicates that the novel proposal is robust against disturbances, thus representing a viable choice for controlling WMRs.

5. Conclusion

This work presented a novel approach for controlling wheeled mobile robots. A disturbance observer was developed to estimate and compensate for internal and external disturbances. Also, a proportional-retarded controller was designed to make the vehicle position and orientation signals converge to a desired reference. A fundamental part of the proposed scheme was developing an efficient methodology that combines the disturbance observer with the delayed controller to attain asymptotic stability in the trajectory-tracking problem. An important advantage of the novel scheme is its ability to diminish the effect of the disturbances. Besides, the experimental results demonstrated the robustness of the novel methodology and its superiority against existing control schemes from the literature. Other advantages of the novel controller include a fast convergence rate, low tracking error, and considering the effect of the disturbance in the controller design stage. The proposed controller's main drawback is the need for velocity measurements by the observer and a more systematic way to select the parameters concerning the controller gains. Hence, future research directions include combining the proposed controller with a disturbance observer without requiring velocity measurements. Also, it can be considered a new design for the proportional retarded controller where a performance index can be selected to obtain appropriate gains for any system. Moreover, it can be considered a modification in the controller structure to attenuate the effect of unmatched

disturbances. Hence, the novel controller developed in this manuscript is an appealing and effective robust control methodology that can be applied to wheeled mobile robots.

CRediT authorship contribution statement

Jesús Abraham Rodríguez-Arellano: Writing – review & editing, Visualization, Validation, Software, Data curation. **Roger Miranda-Colorado:** Writing – review & editing, Writing – original draft, Visualization, Validation, Supervision, Software, Resources, Project administration, Methodology, Investigation, Funding acquisition, Formal analysis, Data curation, Conceptualization. **Raúl Villafuerte-Segura:** Writing – review & editing, Writing – original draft, Software, Methodology, Investigation. **Luis T. Aguilar:** Writing – review & editing, Resources, Funding acquisition.

Declaration of competing interest

The authors declare that they have no known competing financial interests or personal relationships that could have appeared to influence the work reported in this paper.

Acknowledgements

This work received financial support from Secretaría de Ciencia, Humanidades, Tecnología e Innovación, SECIHTI, under the program “Investigadoras e investigadores por México”, Project CIR/063/2024 “Control Robusto para el Control y Reducción de Consumo Energético de Sistemas Mecatrónicos”. This work was also supported by Instituto Politécnico Nacional under Grant SIP 2025-0496. Also, the authors thank to Lorena Citlalli Ledón Morales for her valuable support during the writting of this document.

Appendix A. Supplementary material

Supplementary material related to this article can be found online at https://doi.org/10.1016/j.apm.2025.116038.

Data availability

Data will be made available on request.

References

[1] U. Nehmzow, Mobile Robotics: A Practical Introduction, Springer Science & Business Media, 2012.
[2] L. Jiaxin, et al., Modeling the impact of terrain surface deformation on drag force using discrete element method and empirical formulation, Appl. Math. Model. 136 (2024) 115636, https://doi.org/10.1016/j.apm.2024.115636.
[3] S.G. Tzafestas, Introduction to Mobile Robot Control, Elsevier, 2014.
[4] K. Kanjanawanishkul, Omnidirectional wheeled mobile robots: wheel types and practical applications, Int. J. Adv. Mechatron. Syst. 6 (6) (2015) 289–302, https://doi.org/10.1504/IJAMECHS.2015.074788.
[5] A. Gfrerrer, Geometry and kinematics of the Mecanum wheel, Comput. Aided Geom. Des. 25 (9) (2008) 784–791, https://doi.org/10.1016/j.cagd.2008.07.008.
[6] S.M. Arbatsofla, et al., Fuzzy fractional-order adaptive robust feedback linearization control optimized by the multi-objective artificial hummingbird algorithm for a nonlinear ball–wheel system, J. Braz. Soc. Mech. Sci. Eng. 45 (11) (2023) 575, https://doi.org/10.1007/s40430-023-04455-9.
[7] K. Shabalina, et al., Comparative Analysis of Mobile Robot Wheels Design, in: 2018 11th International Conference on Developments in Esystems Engineering, IEEE, 2018, pp. 175–179.
[8] H. Yu, et al., Finite-time trajectory tracking control of mobile robots based on dynamic terminal sliding mode, in: 2022 34th Chinese Control and Decision Conference (CCDC), IEEE, 2022, pp. 4421–4426.
[9] H. Zhang, et al., Finite-time optimal control for a class of nonlinear systems with performance constraints via critic-only ADP: theory and experiments, Inf. Sci. 690 (2025) 1–16, https://doi.org/10.1016/J.INS.2024.121542.
[10] S. Miao, Y. Zhou, An identical path tracking control strategy of the tractor-trailer wheeled mobile robot with an off-axle hitching based on a passive steering angle, J. Franklin Inst. 361 (4) (2024) 106634, https://doi.org/10.1016/j.jfranklin.2024.01.035.
[11] H.-M. Wu, M.Q. Zaman, Obstacle-aware path following of omni-wheeled robots using fuzzy inference approach, Chaos Solitons Fractals 187 (2024) 115469, https://doi.org/10.1016/j.chaos.2024.115469.
[12] S. Li, et al., Force feedback event triggering-based tracking control for wheeled mobile robots, T-ASE, https://doi.org/10.1109/TASE.2024.3461953, 2024.
[13] W. Zhou, et al., Application of Fuzzy PID Algorithm in Path Control of Intelligent Tracking Vehicles, in: 2024 WRC Symposium on Advanced Robotics and Automation (WRC SARA), IEEE, Beijin, China, August 23, 2024, pp. 423–429.
[14] F. Huo, et al., A new approach to smooth path planning of Ackerman mobile robot based on improved ACO algorithm and B-spline curve, Robot. Auton. Syst. 175 (2024) 1–14, https://doi.org/10.1016/j.robot.2024.104655.
[15] A. Scheuer, T. Fraichard, Planning Continuous-Curvature Paths for Car-Like Robots, in: Proceedings of IEEE/RSJ International Conference on Intelligent Robots and Systems. IROS'96, vol. 3, IEEE, 1996, pp. 1304–1311.
[16] G. Klančar, I. Škrjanc, Tracking-error model-based predictive control for mobile robots in real time, Robot. Auton. Syst. 55 (6) (2007) 460–469, https://doi.org/10.1016/j.robot.2007.01.002.
[17] W. Gu, et al., Trajectory planning and tracking control of a ground mobile robot: a reconstruction approach towards space vehicle, ISA Trans. 87 (2019) 116–128, https://doi.org/10.1016/J.ISATRA.2018.11.019.
[18] A.B. Robat, et al., Dynamics modeling and path following controller of tractor-trailer-wheeled robots considering wheels slip, ISA Trans. 148 (2024) 45–63, https://doi.org/10.1016/j.isatra.2024.03.004.
[19] C. Wang, et al., Formation tracking of multi-robot systems with switching directed topologies based on Udwadia-Kalaba approach, Appl. Math. Model. 126 (2024) 147–158, https://doi.org/10.1016/j.apm.2023.10.035.

[20] M. Korayem, et al., Adaptive robust control with slipping parameters estimation based on intelligent learning for wheeled mobile robot, ISA Trans. 147 (2024) 577–589, https://doi.org/10.1016/j.isatra.2024.02.008.
[21] A. De Luca, et al., Feedback control of a nonholonomic car-like robot, in: J.P. Laumond (Ed.), Robot Motion Planning and Control, in: Lecture Notes in Control and Information Sciences, vol. 229, 1998, pp. 171–253.
[22] H. Ye, S. Wang, Trajectory tracking control for nonholonomic wheeled mobile robots with external disturbances and parameter uncertainties, Int. J. Control Autom. Syst. 18 (12) (2020) 3015–3022, https://doi.org/10.1007/s12555-019-0643-y.
[23] J. Bai, et al., Trajectory tracking control for wheeled mobile robots with kinematic parameter uncertainty, Int. J. Control Autom. Syst. 20 (5) (2022) 1632–1639, https://doi.org/10.1007/S12555-021-0212-Z.
[24] K. Liu, et al., Adaptive sliding mode based disturbance attenuation tracking control for wheeled mobile robots, Int. J. Control Autom. Syst. 18 (5) (2020) 1288–1298, https://doi.org/10.1007/S12555-019-0262-7.
[25] H. Peng, et al., Chance-constrained sneaking trajectory planning for reconnaissance robots, Appl. Math. Model. 112 (2022) 224–237, https://doi.org/10.1016/j.apm.2022.08.009.
[26] E.A. Martínez-García, et al., Directional fields algebraic non-linear solution equations for mobile robot planning, Appl. Math. Model. 38 (21–22) (2014) 5298–5314, https://doi.org/10.1016/j.apm.2014.04.013.
[27] J.A. Rodríguez-Arellano, et al., Prescribed-time trajectory tracking control of wheeled mobile robots using neural networks and robust control techniques, Comput. Sist. 28 (2) (2024) 821–836, https://doi.org/10.13053/cys-28-2-5025.
[28] Z. Li, et al., Adaptive robust coordinated control of multiple mobile manipulators interacting with rigid environments, Automatica 46 (12) (2010) 2028–2034, https://doi.org/10.1016/j.automatica.2010.08.012.
[29] L. Ding, et al., Experimental study and analysis on driving wheels' performance for planetary exploration rovers moving in deformable soil, J. Terramech. 48 (1) (2011) 27–45, https://doi.org/10.1016/j.jterra.2010.08.001.
[30] W.E. Dixon, et al., Tracking and regulation control of a mobile robot system with kinematic disturbances: a variable structure-like approach, J. Dyn. Syst. Meas. Control 122 (4) (2000) 616–623, https://doi.org/10.1115/1.1316795.
[31] D. Wang, C.B. Low, Modeling and analysis of skidding and slipping in wheeled mobile robots: control design perspective, IEEE Trans. Robot. 24 (3) (2008) 676–687, https://doi.org/10.1109/TRO.2008.921563.
[32] S.J. Yoo, B.S. Park, Quantized feedback control strategy for tracking performance guarantee of nonholonomic mobile robots with uncertain nonlinear dynamics, Appl. Math. Comput. 407 (2021) 1–12, https://doi.org/10.1016/j.amc.2021.126349.
[33] C. Laugier, et al., Sensor-based control architecture for a car-like vehicle, Auton. Robots 6 (1999) 165–185, https://doi.org/10.1023/A:1008835527875.
[34] R. Lenain, et al., Adaptive Control for Car Like Vehicles Guidance Relying on RTK GPS: Rejection of Sliding Effects in Agricultural Applications, in: 2003 IEEE International Conference on Robotics and Automation (Cat. No. 03CH37422), vol. 1, in: IEEE, Taipei, Taiwan, 14-19 September, 2003, pp. 115–120.
[35] C.-H. Sun, et al., Sequentially switched fuzzy-model-based control for wheeled mobile robot with visual odometry, Appl. Math. Comput. 47 (2017) 765–776, https://doi.org/10.1016/j.apm.2016.11.001.
[36] R. Miranda-Colorado, Observer-based finite-time control for trajectory tracking of wheeled mobile robots with kinematic disturbances, ISA Trans. 148 (2024) 64–77, https://doi.org/10.1016/j.isatra.2024.03.031.
[37] H. Zhang, et al., Nonsingular recursive-structure sliding mode control for high-order nonlinear systems and an application in a wheeled mobile robot, ISA Trans. 130 (2022) 553–564, https://doi.org/10.1016/j.isatra.2022.04.021.
[38] L.D. Fufa, E. Ayenew, Trajectory tracking of a two-wheeled mobile robot using backstepping and nonlinear PID controller, in: International Conference on Advances of Science and Technology, Springer, 2022, pp. 290–304.
[39] L. Zhao, et al., Double-loop tracking control for a wheeled mobile robot with unmodeled dynamics along right angle roads, ISA Trans. 136 (2023) 525–534, https://doi.org/10.1016/j.isatra.2022.10.045.
[40] D. Wang, et al., Sliding mode observer-based model predictive tracking control for mecanum-wheeled mobile robot, ISA Trans. 151 (2024) 51–61, https://doi.org/10.1016/j.isatra.2024.05.050.
[41] W. Yuan, et al., Differential flatness-based adaptive robust tracking control for wheeled mobile robots with slippage disturbances, ISA Trans. 144 (2024) 482–489, https://doi.org/10.1016/j.isatra.2023.11.008.
[42] L. Yan, et al., Trajectory tracking control of nonholonomic wheeled mobile robots using only measurements for position and velocity, Automatica 159 (2024) 111374, https://doi.org/10.1016/j.automatica.2023.111374.
[43] L. Liu, et al., Comparative study of adaptive trajectory tracking controller for four-wheel mobile robot with prescribed-prediction performance, Control Eng. Pract. 152 (2024) 106076, https://doi.org/10.1016/j.conengprac.2024.106076.
[44] H. Xiao, et al., Reinforcement learning-driven dynamic obstacle avoidance for mobile robot trajectory tracking, Knowl.-Based Syst. 297 (2024) 111974, https://doi.org/10.1016/j.knosys.2024.111974.
[45] A. Rosas-Vilchis, et al., Trajectory tracking control for an autonomo vehicle using a decoupling approach, in: 2020 28th Mediterranean Conference on Control and Automation (MED), IEEE, 2020, pp. 375–380.
[46] J.-X. Zhang, et al., Fault-tolerant prescribed performance control of wheeled mobile robots: a mixed-gain adaption approach, IEEE Trans. Autom. Control (2024), https://doi.org/10.1109/TAC.2024.3365726.
[47] Q. Lu, et al., Practical fixed-time trajectory tracking control of constrained wheeled mobile robots with kinematic disturbances, ISA Trans. 129 (2022) 273–286, https://doi.org/10.1016/j.isatra.2021.12.039.
[48] W. Ding, et al., Adaptive fuzzy control of wheeled mobile robots with prescribed trajectory tracking performance, IEEE Trans. Fuzzy Syst. (2024), https://doi.org/10.1109/TFUZZ.2024.3401691.
[49] C. Zhu, et al., Trajectory tracking control of car-like mobile robots based on extended state observer and backstepping control, Electronics 13 (8) (2024) 1563, https://doi.org/10.3390/electronics13081563.
[50] U. Kiencke, A. Daiß, Observation of lateral vehicle dynamics, Control Eng. Pract. 5 (8) (1997) 1145–1150, https://doi.org/10.1016/S0967-0661(97)00108-1.
[51] O. Ljungqvist, et al., A path planning and path-following control framework for a general 2-trailer with a car-like tractor, J. Field Robot. 36 (8) (2019) 1345–1377, https://doi.org/10.1002/rob.21908.
[52] M. Hussein, et al., Distributed fault-tolerant formation control design via high-order sliding mode for a team of car-like vehicles, IEEE Trans. Intell. Veh. (2023), https://doi.org/10.1109/TIV.2023.3340549.
[53] C. Abdallah, et al., Delayed positive feedback can stabilize oscillatory systems, in: Proceedings of the 1993 American Control Conference (ACC), IEEE, 1993, pp. 3106–3107.
[54] H. Suh, Z. Bien, Use of time-delay actions in the controller design, IEEE Trans. Autom. Control 25 (3) (1980) 600–603, https://doi.org/10.1109/TAC.1980.1102347.
[55] S.-I. Niculescu, et al., Some remarks on the delay stabilizing effect in SISO systems, in: Proceedings of the 2003 American Control Conference, 2003 (ACC), vol. 3, in: IEEE, Denver, CO, USA, 04-06 June, 2003, pp. 2670–2675.
[56] R. Villafuerte, et al., Proportional retarded control of a second order system, in: 2009 6th International Conference on Electrical Engineering, Computing Science and Automatic Control (CCE), IEEE, 2009, pp. 1–6.
[57] R. Villafuerte-Segura, Delayed controllers for time-delay systems, Commun. Nonlinear Sci. Numer. Simul. 117 (2023) 106934, https://doi.org/10.1016/j.cnsns.2022.106934.

[58] G. Oaxaca-Adams, R. Villafuerte-Segura, On controllers performance for a class of time-delay systems: maximum decay rate, Automatica 147 (2023) 110669, https://doi.org/10.1016/j.automatica.2022.110669.
[59] R. Villafuerte-Segura, et al., Observer-based proportional-retarded controller for payload swing attenuation of 2D-crane systems including load hoisting-lowering, ISA Trans. (2024), https://doi.org/10.1016/j.isatra.2024.09.022.
[60] A. Ramírez, R. Sipahi, Multiple intentional delays can facilitate fast consensus and noise reduction in a multiagent system, IEEE Trans. Cybern. 49 (4) (2018) 1224–1235, https://doi.org/10.1109/TCYB.2018.2798163.
[61] S.J. Yoo, Adaptive neural tracking and obstacle avoidance of uncertain mobile robots with unknown skidding and slipping, Inf. Sci. 238 (2013) 176–189, https://doi.org/10.1016/j.ins.2013.03.013.
[62] H. Rios, et al., Continuous sliding-modes control strategies for quad-rotor robust tracking: real-time application, IEEE Trans. Ind. Electron. 432 (2019) 1264–1272, https://doi.org/10.1109/TIE.2018.2831191.
[63] J.-H. Park, et al., Asymptotically convergent switching differentiator, Int. J. Adapt. Control Signal Process. 33 (3) (2019) 557–566, https://doi.org/10.1002/acs.2969.
[64] J.I. Neimark, D-decomposition of the space of quasi-polynomials (on the stability of linearized distributive systems), Am. Math. Soc. Transl. 102 (1973) 95–131.
[65] K. Gu, et al., Stability of Time-Delay Systems, Springer Science & Business Media, 2003.
[66] C.-I. Morarescu, S. Niculescu, Stability crossing curves of SISO systems controlled by delayed output feedback, Dyn. Contin. Discrete Impuls. Syst., Ser. B, Appl. Algorithms 14 (5) (2007) 659–678.
[67] G. Oaxaca-Adams, et al., On non-fragility of controllers for time delay systems: a numerical approach, J. Franklin Inst. 358 (9) (2021) 4671–4686, https://doi.org/10.1016/j.jfranklin.2021.03.030.
[68] AutoMiny, Autominy webpage, https://autominy.github.io/AutoMiny/, 2025. (Accessed February 2025).
[69] O. Robotics, Ros distibutions and information, https://wiki.ros.org/Distributions, 2025. (Accessed February 2025).
[70] C. Ltd, Ubuntu information, https://ubuntu.com/tutorials/install-ubuntu-desktop#1-overview, 2025. (Accessed February 2025).
[71] J.A. Rodríguez-Arellano, et al., Trajectory tracking nonlinear H_∞ controller for wheeled mobile robots with disturbances observer, ISA Trans. 142 (2023) 372–385, https://doi.org/10.1016/j.isatra.2023.07.037.
[72] R. Miranda-Colorado, Observer-based proportional integral derivative control for trajectory tracking of wheeled mobile robots with kinematic disturbances, Appl. Math. Comput. 432 (2022) 127372, https://doi.org/10.1016/j.amc.2022.127372.
[73] J.A. Rodríguez-Arellano, et al., Autominy experiments, https://drive.google.com/file/d/1WIqAAOJK3EFkTsCZUX84PDrfMB8pb5Zi/view?usp=sharing, 2025. (Accessed February 2025).